SANDIA REPORT

SAND91—0105 • UC—~~251~~902
Unlimited Release
Printed July 1991

Interim Report on the Effects of Brine-Saturation and Shear Stress on Consolidation of Crushed, Natural Rock Salt from the Waste Isolation Pilot Plant (WIPP)

David H. Zeuch, Daniel J. Zimmerer, Marlene E. F. Shields

Prepared by
Sandia National Laboratories
Albuquerque, New Mexico 87185 and Livermore, California 94550
for the United States Department of Energy
under Contract DE-AC04-76DP00789

Issued by Sandia National Laboratories, operated for the United States Department of Energy by Sandia Corporation.

Available to DOE and DOE contractors from
Office of Scientific and Technical Information
PO Box 62
Oak Ridge, TN 37831

Prices available from (615) 576-8401, FTS 626-8401

Available to the public from
National Technical Information Service
US Department of Commerce
5285 Port Royal Rd
Springfield, VA 22161

NTIS price codes
Printed copy: A04
Microfiche copy: A01

SAND--91-0105

DE91 018624

Interim Report on the Effects of Brine–Saturation and Shear Stress on Consolidation of Crushed, Natural Rock Salt from the Waste Isolation Pilot Plant (WIPP)

by

David H. Zeuch, Daniel J. Zimmerer and Marlene E. F. Shields
Geomechanics Division 6232
Sandia National Laboratories
Albuquerque, NM 87185

Abstract

The mechanical behavior of crushed natural rock salt is of concern to the Waste Isolation Pilot Plant (WIPP) Project because excavated salt is a candidate material for use as backfill around the waste packages and in storage rooms, shafts and other underground openings. To complement existing studies on the compaction behavior of dry and damp (*i.e.,* unsaturated) crushed rock salt under hydrostatic compression, we initiated an extensive experimental program to evaluate (1) the effect of brine–saturation on the consolidation rates and terminal densities of crushed salt subjected to hydrostatic compression, and (2) the influence of small deviatoric stresses on the consolidation rate of damp crushed rock salt. This investigation is far from complete, but our experiments necessarily run for extended periods (up to 11 months) and laboratory facilities are limited. Therefore, in this report we review such results as are now in hand, in order to make available preliminary *estimates* of the effects of brine–saturation and shear stress on consolidation. Experiments with brine were carried out under nominally drained conditions. Experiments completed to date include five hydrostatic compaction tests on brine–saturated samples, run at pressures ranging from 1.72 to 10.34 MPa, and two prototype shear consolidation experiments run at a mean stress of 3.45 MPa and a stress difference of 0.69 MPa. Both sets of experiments were run at 20±0.5 °C. Although the experiments on brine–saturated crushed rock salt exhibit several discrepancies, we can draw the following conclusions. (1) Though effects associated with brine–saturation apparently have a retarding effect on consolidation, rates are reduced by less than an order of magnitude when compared with unsaturated specimens; specifically, at comparable pressures unsaturated specimens compact 2.5 to 6 times faster than brine–saturated samples. (2) Despite saturation, high fractional densities (>0.95) are attainable even on laboratory time scales using pressures well below lithostatic at the WIPP (≈15 MPa). Results for the two shear–consolidation experiments are disparate, with one experiment suggesting that shear stress slightly accelerates consolidation, while the other suggests that it may inhibit consolidation. If we conservatively assume that the latter is true, then the available results suggest that, at worst, rates are retarded by less than an order of magnitude.

THIS PAGE INTENTIONALLY LEFT BLANK

1 Introduction and Background

The Waste Isolation Pilot Plant (WIPP) is a U.S. Department of Energy research and development facility intended to demonstrate the safe geologic disposal of transuranic wastes. The facility is located approximately 40 km east of Carlsbad in southeastern New Mexico. Underground workings at the WIPP are situated at a depth of about 650 m in a halite–rich horizon of the Salado Formation, part of a 1000–m thick sequence of bedded evaporites.

Mechanical behavior of crushed rock salt is of interest to the WIPP Project because the mined salt (referred to hereafter as "WIPP salt") is a candidate material for use as backfill around the waste packages and in the underground openings during and after the operational phase. It is anticipated that in response to the convergence of the mine openings, the crushed salt will compact sufficiently to serve as an effective component in WIPP seal systems. Desirable features of a long–term seal material will almost certainly be low permeability, and geochemical and mechanical compatibility with the surrounding, intact formation.

As a consequence, a number of studies have been performed at Sandia National Laboratories and elsewhere on the time–dependent compaction behavior of salt of varying degrees of purity, under both dry and wet conditions. A comprehensive review of existing work is beyond the scope of this report. For full compilations and discussions of the literature, the reader is referred to Holcomb and Hannum [1982], Holcomb and Shields [1987], Holcomb and Zeuch [1988; 1990], and Zeuch [1989a; 1990]. In this report, we focus on two specific aspects of the salt consolidation problem, *viz.*, the effect of brine–saturation on hydrostatic compaction of crushed WIPP salt, and the influence of small applied shear stresses on the consolidation of "damp" (*i.e.*, unsaturated) crushed salt. We use only selected references to provide background and motivation for the current experimental investigation.

Holcomb and Hannum [1982] conducted quasistatic and creep compaction tests under hydrostatic pressure on nominally dry crushed natural rock salt obtained from the WIPP site, and on similar material obtained from a nearby, commercially–operated mine. The creep consolidation rates were found to be extremely low. Based on extrapolation of their empirical model for consolidation, Holcomb and Hannum [1982] concluded that unacceptably long times were required to attain the low porosity necessary for the backfill to attain a permeability approaching that of the surrounding formation. Zeuch [1989a; 1990] and Holcomb and Zeuch [1988; 1990] have since developed a more realistic micromechanical compaction model based upon the well–documented power–law expression for dislocation creep of WIPP salt [Wawersik and Zeuch, 1986]. This

model accurately predicts the compaction rates observed in laboratory experiments on dry, crushed salt, beyond approximately one hour after pressure application. Extrapolations based on the model for dry, crushed salt suggest that compaction will continue at rates that are sufficient to reduce the porosity to an acceptable value within about thirty years. The definitive experiments necessary to validate the model remain to be done.

However, the bedded evaporites of the Salado formation contain both inter– and intragranular brine inclusions, which comprise 0.1–1 wt% of the rock [Nowak *et al.*, 1988]. Influx of small quantities of brine into the mine openings is inevitable [Nowak *et al.*, 1988], and the crushed salt backfill will therefore be damp, not dry. Holcomb and Shields [1987] have evaluated the influence of the addition of small amounts of water (approximately 0.5 to 3 wt%) on the compaction rate of crushed WIPP salt under hydrostatic pressures. The pronounced effect of water on the consolidation rate of sodium chloride has been known at least since the work of Kingery *et al.* [1963], so it came as no surprise that the addition of even these small quantities of water accelerated the consolidation rates by approximately two orders of magnitude. Experimental studies on the consolidation of brine–saturated, pure sodium chloride indicate that some form of solution–reprecipitation creep is responsible for acceleration of the densification rate, but the precise mechanism remains unknown [Shor *et al.*, 1981; Raj, 1982; Spiers and Schutjens, 1990]. Holcomb and Shields [1987] developed another entirely empirical model for consolidation of damp crushed salt, and concluded that the backfill probably would compact about as rapidly as the mine walls converge. Subsequent modeling work supports this contention [Sjaardema and Krieg, 1987].

Both observations and calculations indicate that the total influx of brine into the underground openings will be small. It is expected that by the time the crushed salt backfill is fully reconsolidated ($\approx$ 100 years), only 1.2 wt% of the rock mass will consist of trapped brine [Nowak *et al.*, 1988]; this is not much greater than the original brine content of the intact formation. Nevertheless, some concern exists that large quantities of brine might somehow unexpectedly saturate the crushed salt backfill during the early stages of consolidation, and prevent the attainment of final densities approaching those of the intact formation. Even though such a "worst–case" scenario is thought to be extremely unlikely [Nowak *et al.*, 1988] we have undertaken an experimental investigation of the effects of high degrees of brine–saturation on the consolidation rates of crushed WIPP salt under hydrostatic compression.

Tests were conducted under nominally drained conditions at pressures of 1.72, 3.45, 6.90 and 10.34 MPa (250, 500, 1000 and 1500 psi), comparable to those used by Holcomb and Shields [1987], to permit direct comparison between experiments. Our results to date suggest that saturation–related effects may reduce rates of consolidation some-

what, but that high fractional densities (in excess of 0.95) are nevertheless attainable on laboratory time scales for hydrostatic pressures below the lithostatic pressure at the WIPP site. Because effects associated with saturation apparently do inhibit densification, and because it was important to demonstrate the ability to attain high fractional densities, the tests required long durations (up to eleven months) and our data set is small: only five completed experiments are discussed herein. Additional experiments are planned, both at Sandia National Laboratories and elsewhere. Our experience in the laboratory has also suggested some modifications and improvements to our experimental technique. We emphasize that the results presented here are preliminary, and subject to revision. However, the acquisition of further data is still approximately 18 months away; we therefore felt it important to present our interim results and conclusions for use in ongoing analyses by others involved in the WIPP Project.

We also initiated an experimental investigation of the effects of small deviatoric compressive stresses on consolidation of crushed WIPP salt. Numerical simulations of disposal–room/backfill interactions indicate that pressure will not be hydrostatic during compaction, and that the backfill will therefore be subjected to small shear stresses, principally in the corners of drifts [Sjaardema and Krieg, 1987]. Shear stresses are generally believed to enhance the compaction of granular or porous media (*e.g.*, Johnson and Green [1976]); nevertheless, the concern arises that these shear stresses may somehow impede consolidation rates of crushed salt. We report here on the results of two prototype "shear–consolidation" experiments on damp, crushed WIPP salt. The tests were done at mean stresses, $\sigma_m = (\sigma_1 + 2\sigma_3)/3$, of approximately 3.45 MPa, where σ_1, σ_2 and σ_3 are the greatest, intermediate and least principal compressive stresses; in our test geometry $\sigma_2 = \sigma_3$. Results from these two experiments are divergent, and the conclusions that may be drawn from them are limited and preliminary. However, the results from these two tests constitute our only information available regarding the effects of shear stress on consolidation, so we present the results for use in ongoing studies until clearer results are obtained. At this time, the data suggest that small stress differences ($\sigma_1 - \sigma_3 \approx 0.69$ MPa), at worst, retard consolidation rates by about an order of magnitude, but may actually accelerate them relative to the hydrostatic condition. Further shear–consolidation experiments, using the techniques developed in these two prototype tests, will be performed both at Sandia and elsewhere to resolve this discrepancy.

In this report we concentrate strictly on presentation of our results and comparison of our data with those of Holcomb and Shields [1987]. Experiments intended to illuminate the micromechanisms of consolidation of damp or saturated crushed rock salt are planned for the future [Wawersik, 1988; Zeuch, 1989b]. Detailed discussion of experimental and theoretical studies of the micromechanics of consolidation is deferred until then.

2 Experimental Procedures

2.1 Specimen Materials and Construction

The chemistry and mineralogy of rock salt from the WIPP stratigraphic horizon are described elsewhere and will not be reviewed here beyond noting that the rock consists principally of halite, but, on average, contains up to 5 wt% non–halite minerals including quartz, anhydrite, gypsum, magnesite, polyhalite and clays, as well as traces of alkali feldspar and zeolites [Stein, 1985]. Atomic absorption and microprobe studies suggest that the halite phase contains Ca, Mg, and K in solid solution in concentrations exceeding several thousand parts per million. However, low resolution and the ubiquitous presence of secondary phases have, thus far, made it impossible to unequivocally identify impurities in solid solution [Wawersik and Zeuch, 1986]. The possible impact of both secondary phases and solid–solution impurities on dislocation creep of dry, natural rock salt have been discussed elsewhere [Wawersik and Zeuch, 1986; Heard and Ryerson, 1986]. It is interesting to note, however, that the presence of secondary phases may also have some bearing on fluid–phase enhanced creep and compaction of rock salt beyond the effects related to brine–chemistry [Hickman and Evans, in press].

Our procedures for sample construction closely parallel those developed by Holcomb and Hannum [1982] and Holcomb and Shields [1987], after whom this discussion follows. The crushed WIPP salt used to prepare test specimens for this investigation was from the latter of two batches of mine–run material used by Holcomb and Shields [1987], referred to in that study as the "post–December, 1986 batch." The salt was obtained from a mine face at the WIPP site. The continuous miner used at the WIPP facility generates particle sizes up to several centimetres. Owing to the limited dimensions of the salt columns in our sample assemblies (10.2 cm in diameter by 15.2 cm long for hydrostatic tests, and 8.9 cm in diameter by 12.7 cm long for shear–consolidation runs), the mine–run material was sieved to remove all particles that could not pass through a 0.96 cm mesh. The resulting stock material was stored in large plastic bags in the laboratory, taking no special precautions to control moisture content, which Holcomb and Shields [1987] have determined to be 0.19 wt%. Two recent particle size distribution analyses (Figure 1) confirm that the distribution remains essentially identical to that used by Holcomb and Shields [1987].

As mentioned above, two different sample sizes were used. Apart from dimensional differences, however, samples used in the hydrostatic and shear–consolidation experiments were identical. Following Holcomb and Shields [1987], samples were assembled using a double jacket of lead sheet and Viton, sealed by O–rings to vented, hardened stainless steel endcaps of either 10.2 or 8.9 cm (4.1 or 3.5 in) in diameter (Figure 2). Lead sheet

(approximately 2 mm thick) was formed into a cylinder with an inner diameter corresponding to the diameter of the endcap appropriate to the type of experiment, 10.2 or 8.9 cm. Height of the lead cylinder for the larger, hydrostatic compaction experiments was 20.3 cm, while for the smaller shear–consolidation experiments the height was 19 cm. The seam in the lead cylinder was soldered to create a smooth edge, and to provide rigidity during sample assembly. The outer Viton jacket served as the actual pressure seal. The function of the lead liner was to prevent the Viton jacket from puncturing as it deformed into the uneven, dimpled surface of the compacting salt. To further reduce the possibility of jacket ruptures we used an intermediate face plate of aluminum with a broadly beveled edge to eliminate a sharp offset at the salt/endcap interface [Holcomb and Shields, 1987]. The intermediate endcap was drilled through with a 1.5 mm hole to permit escape of brine and gases during compaction. A thin (0.157 cm–thick) disk of felt metal was inserted between the aluminum and steel endcaps to prevent salt from plugging the small vent hole in the steel endcap. (In current experiments, we have moved the felt metal to the interface between the salt and the aluminum face plate.) Partial sample assembly was necessary before the salt could be added. One end of the lead/Viton cylinder was plugged by an endcap assembly (tapered aluminum spacer, felt metal, stainless steel endcap and O–rings) of appropriate diameter. The Viton jacket was sealed around the O–rings using twisted wire wrappings. In the case of brine–saturated experiments, the basal endcap vent was plugged. Salt could then be added to this partially–constructed cylinder.

Prior to addition of the crushed salt, the mass and volume of the sample assembly components were determined for later use in calculating the volume strain and fractional density of the sample. Mass was determined using a digital Metler balance, accurate to 0.1 g and calibrated annually against known standards. Volume measurements were made using the fluid–displacement method, but two different techniques were used to determine the change in height of liquid in a large, clear plastic cylinder. For most of this investigation, we have used an older technique developed by Holcomb and Hannum [1982] and Holcomb and Shields [1987]. The technique relied on visual measurement of the change in height of the fluid column using a height gauge and a horizontally–projected laser beam on a precision, vertically–adjustable mount. We have determined that measurements against a known standard having a volume comparable to the salt assemblies are accurate and repeatable within $\pm$ 24 cm^3, twice the standard deviation of repeated measurements. This corresponds to a possible error in our measured fractional densities of approximately $\pm$ 0.02. During this study we modified this method by mounting the barrel of a linear variable differential transformer (LVDT) vertically on the inner edge of the plastic cylinder and mounting the LVDT core on a float on the surface of the water in the cylinder. Measurements against the same known standard are accurate and repeatable within ± 7 cm^3.

To build the salt column, an excess quantity of crushed salt was poured onto a clean surface in a conical heap. The pile was then divided into eight roughly equal wedges, which were successively poured into the partially–constructed lead/Viton cylinder until a height of 15.2 or 12.7 cm was reached. The purpose of this procedure was to ensure a uniform particle size distribution throughout the specimen. For both types of test, measured quantities of saturated brine were added along with the salt in 8–10 equal aliquots, resulting in a final brine content known to be less than 2.5 wt% of the specimen. At this point, the partial sample assembly, salt and brine were weighed, in order to determine the mass of the salt. Any additional brine needed to bring the content to 2.5 wt% was added at this time. Sample construction was then completed by addition of another aluminum spacer, felt metal disc and steel endcap. The upper endcap was also sealed around the O–ring using twisted wire. Volume measurements were then performed on the complete sample assembly. By subtracting out the predetermined volume of the non–salt components, and knowing the mass of the salt, the initial volume (V_0) and initial fractional density (D_0) of the crushed salt could be determined. Fractional density is a dimensionless quantity defined as the ratio of the sample density to that of the void–free solid, 2.14 g cm^{-3} for intact WIPP salt [Holcomb and Hannum, 1982; Holcomb and Shields, 1987]. By referring the sample density to that of intact WIPP salt we have, in effect, treated the brine as a massless quantity occupying only void space and totally free to escape. Our fractional density, so defined, is then a measure of the extent to which brine is expelled and the test specimens once again become "dry," solid masses of salt.

Direct volume measurements were performed using the immersion method at various times during an experiment: immediately following specimen assembly, as outlined in the preceding paragraph; immediately following preconditioning at the beginning of a new pressure stage (see below); and at the termination of a pressure stage. Each time a measurement was performed, it was necessary to evacuate the specimen to remove air trapped between the Viton and lead jackets, though this problem was noticeably most troublesome for the first volume measurement prior to any preconditioning or creep consolidation; for this reason, volume measurements performed later in the experiment are probably more reliable. The problem was compounded by the high degree of specimen saturation. Prolonged efforts to draw a vacuum on the specimens inevitably resulted in removal of water from the specimens; thus, it was necessary to keep evacuation times to a minimum, stopping as soon as the Viton jacket was visibly drawn up tightly against the lead liner. Our inability to assess the consistency with which specimens were evacuated from time to time introduces a possible error in the volume measurement the size of which is impossible to estimate. We believe that it is small, however, because air trapped within the Viton jacket in excess of a few cubic centimetres would be visually detectable.

For hydrostatic compaction experiments on brine–saturated specimens, this completed sample assembly. For shear–consolidation experiments, one additional step was necessary. In order to maintain a constant stress difference, and, hence, shear stress on the test specimen, the change in cross–sectional area of the sample must be known. Assuming isotropic lateral compaction, this change can be calculated from the loading piston displacement and dilatometric measurements (discussed below). Nevertheless, we deemed it important to compare direct measures of change in sample diameter with calculated values until experience and confidence were developed in this new type of experiment.

In the first of our two prototype experiments, a LVDT displacement gauge [Holcomb and McNamee, 1984] was mounted midway along the length of the cylindrical sample in order to monitor the decrease in sample diameter with densification. Though this technique was largely successful, the bulkiness of the displacement gauge combined with the limited diametral working space in the pressure vessel made test set–up extremely difficult. In addition, the limited linear range of the miniature LVDTs (0.254 cm, or 0.1 in) made measurements in the later stages of the test doubtful. In the second prototype experiment, two "disk gauges" [Schuler, 1979] were mounted across perpendicular diameters at distances about one–third of the height of the salt column from either endcap assembly (Figure 3). The mounting/adjusting screws that make contact with the Viton jacket were mounted against small squares of copper sheet that were glued to the jacket. The copper sheet prevented jacket punctures and, we believe, helped to average out the local variability in sample diameter caused by uneven compaction of the granular salt. No evidence of detachment of the copper sheet from the jacket was detected at the end of the test.

The disk gauges are relatively compact and, having large linear ranges, are well–suited to measurement of large strains. This method proved to be both straightforward and successful. Because it is relatively easy to do, the technique will be continued in future experiments, ensuring a backup measurement for the calculated value of diametral change. Though the surface of the salt dimples during densification, we have found that post–test, averaged point contact measurements agree quite well with values obtained from disk gauges for change in sample diameter (see below).

Irrespective of whether LVDT displacement or disk gauges were used, the initial sample diameter and length were measured at several randomly chosen points before the start of the test. Knowing the thicknesses of the lead and Viton jackets, as well as the thickness of the endcap assemblies, changes in loading piston position (see below) and changes in LVDT displacement or disk gauge readings could be converted to current sample length and diameter for comparison with the dilatometric data.

2.2 Testing Apparatus and Procedures

2.2.1 Hydrostatic Compaction Experiments

The test apparatus used for the hydrostatic compaction experiments in this study was developed by W. R. Wawersik. Because it has been described elsewhere in detail, as used both in testing of intact rock [Wawersik and Preece, 1984] and for compaction experiments on crushed salt [Holcomb and Hannum, 1982; Holcomb and Shields, 1987], only the barest of descriptions will be presented. The system remains virtually unchanged since the work of Holcomb and Shields [1987], so our resolution and estimated errors for measured and calculated quantities are comparable to those of the earlier study. All testing was done in a temperature–controlled room kept at 20±0.5°C.

The apparatus consists of a 69 MPa (10,000 psi) pressure vessel and a 0.444 MN (100,000 lbs) hydraulic actuator, mounted in a reaction frame that permits transfer of force from the hydraulic actuator to a cylindrical test specimen within the vessel (Figure 4). The test specimen can thus be subjected to deviatoric, as well as hydrostatic loading. Deviatoric loading is controlled by either a 0.02 m^3 (5 gal) accumulator or an electrohydraulic pump. Changes in the position of the loading piston, and hence, axial deformation of the test specimen, are indicated by externally–mounted LVDTs. Force on the loading piston is measured by an externally–mounted load cell in the loading column. True–stress tests are effected by manual updates on the force necessary to keep stress constant on the sample's changing cross–sectional area. Diametral changes in the sample can be calculated from the externally–measured axial deformation assuming homogenous strain, or measured directly using one of a variety of internal, clip–on gauges. In hydrostatic compaction experiments, the hydraulic actuator was valved off, locked in place and used only to seal the vessel, though both force on, and position of, the loading piston were monitored.

Confining pressure is applied by a separate hydraulic system, consisting of a hand pump and a servocontrolled, screw–driven intensifier/dilatometer. Pressure is controlled within ±0.01 MPa (2 psi) by comparing the voltage output from a standard pressure transducer with a reference voltage representing the desired pressure. A DC stepping motor drives the intensifier piston in or out, and, hence, the pressure up or down, in response to differences outside of preset, adjustable limits. The intensifier also serves as a dilatometer; that is, it is used to measure specimen volume changes during the experiment. At constant pressure, any changes in the volume of silicone oil necessary to maintain the pressure constant can be attributed to changes in the sample volume. A multiturn potentiometer is coupled to the rotating shaft of the intensifer, such that changes in volume in the intensifier piston can be directly related to a voltage

change. System resolution has been estimated at about 0.01 cm^3 [Holcomb and Shields, 1987].

Specimens up to 10.2 cm (4.1 in) in diameter by 21 cm (8.25 in) long may be accommodated in the pressure vessel. Though all of our experiments were performed at 20±0.5°C, the apparatus is equipped with heaters that permit testing at temperatures up to 250°C.

In a typical hydrostatic experiment, the sample was initially compacted, or "conditioned," in the pressure vessel using only the hand pump. The specimen was quickly raised to the desired test pressure (no higher), and then held at pressure for approximately one minute. The sample was then removed from the vessel and the "instantaneous," or quasistatic volume change ΔV_q determined by the immersion method. This procedure follows that of Holcomb and Hannum [1982] and Holcomb and Shields [1987] who found that the dilatometer system could not be reliably used to determine the initial volume change owing to the (1) large volume change, (2) the dependence of oil volume on pressure, and, (3) cooling following adiabatic heating of the oil during pressurization. Several of our experiments were run at successively higher pressures. Each new pressure stage was preceded by conditioning and direct volume measurement. When necessary, we also removed the endcaps and cleaned the felt metal disks and endcap vents to remove trapped salt that might slow the escape of brine and impede consolidation.

After the initial compaction, the specimens were saturated with brine insofar as possible. The upper endcap assembly was removed and measured quantities of pre–saturated brine solution were allowed to imbibe into the sample for a period of twelve hours. Knowing the initial and quasistatic fractional densities, void space and degree of saturation could therefore be estimated. In no case did we attain 100% saturation; the values ranged from 83 to 96% (Table 3). Whether "complete" saturation could have been accomplished is unknown. In addition to the fact that we had no way to know how much of the estimated void space was *connected*, we found that attempts to increase saturation by imbibation beyond about twelve hours resulted in incipient disaggregation of the specimen, which, if allowed to continue would render meaningless our direct, post–conditioning volume measurement. We were thus forced to settle for less than complete saturation in order to retain meaningful estimates of degree of saturation and current specimen volume. We presume that disaggregation was caused by preferential dissolution (and concurrent reprecipitation elsewhere) of highly–stressed, plastically–deformed interparticle contacts. This type of dissolution–reprecipitation will occur even in a brine–saturated solution because the free energy of the system is reduced by elimination of the intracrystalline elastic strain energy caused by high dislocation densities (*e.g.*, Bosworth [1981]).

After twelve hours of imbibation, the endcap was replaced, the jacket sealed, and the sample returned to the pressure vessel. The specimen was rapidly repressurized to the test pressure, and the dilatometer/intensifier turned on to measure the time–dependent volume change (ΔV_c). Though the lower endcap vent was plugged to prevent drainage of the brine from the specimen under the influence of gravity, brine was permitted to drain from the upper ported endcap into a graduated cylinder. The cylinder was capped to prevent evaporation of brine, and the amount of brine expelled was logged on a regular basis throughout the experiment. In the future, volumes of both brine and escaping air (if any) will be monitored regularly. We observed that where estimates of saturation were high (*e.g.*, **09JU88** and **08MR89**, estimated at 96 and 90% of saturation), volumes of brine expelled were within a few cubic centimetres of the volume changes measured by either immersion or dilatometry during the creep consolidation stages (*cf.* Table 2). Where estimated saturations were somewhat lower (*e.g.*, **24JL71** and **20SE89**, estimated at 87 and 83%), agreement between volumes of brine expelled and volume changes measured by immersion or dilatometry were correspondingly poorer.

Tests ran for up to eleven months. At the termination of an experiment, a direct volume measurement was made to determine the final fraction density. Specimens from several of the completed experiments discussed here have been sealed and preserved for brine–permeability measurements. At the conclusion of those measurements, the specimens will be cored, measured, weighed and dried, for more precise determinations of fractional density and water content. Some of the specimens may also be used for microstructural studies.

2.2.2 Shear–Consolidation Experiments

The "creep bench" apparatus used for the two prototype shear–consolidation experiments was also designed by W. R. Wawersik, and is fundamentally similar to those used for the hydrostatic compression tests. The two apparatuses have comparable sample size, temperature and confining pressure capabilities. Similarly, position of the axial loading piston is monitored by LVDTs, and pressure and load are measured using standard pressure and load cells. The apparatuses differ principally in the design of the reaction frame, maximum load capability, availability of high–pressure electrical feedthroughs, and method for control of the confining pressure and axial load. The first two differences are unimportant in relationship to this study. Each creep bench pressure vessel is equipped with twelve high pressure feedthroughs, and this was important to our ability to use displacement and disk gauges inside the pressure vessel, attached directly to the specimen. Finally, on the creep bench both axial load and confining

pressure are servocontrolled, and this will eventually be important to our ability to automate axial load updates as the cross–sectional area decreases during consolidation.

On the creep bench, control units compare amplified signals from the pressure and load cells with a reference voltage corresponding to the desired pressure or load. When pressure or load fall outside of preset, adjustable limits, the controllers open fast–operating, air–activated valves which either: (1) admit hydraulic oil from a high–pressure reservoir and increase the pressure or load, or (2) drain oil, lowering the pressure or load. Because we required dilatometric capability for our shear–consolidation experiment, we bypassed the creep bench's servocontrolled confining pressure system and installed a dilatometer/intensifier identical to those used in the hydrostatic compression experiments. However, we did make use of the servocontrolled load capability. In our first experiment, we used the servocontroller to keep load constant between manual updates, that is, lowering the load in response to calculated reductions in cross–sectional area caused by compaction. In the second experiment we included a microprocessor–based controller in the control loop. In this configuration, the output signals from the loading piston LVDT, dilatometer and disk gauges were input to the microprocessor. Using these data, the microprocessor calculated the new cross–sectional area, and correspondingly adjusted the reference voltage input to the controller, lowering the axial force on the specimen. This testing configuration was only partially successful (see below) but modifications are planned which should improve our control.

Tests were run similarly to the hydrostatic compaction experiments, though no brine was added beyond the approximately 2.5 wt% water added during the sample assembly. The specimens were conditioned for approximately one minute at a hydrostatic pressure corresponding to the mean stress to be employed in the experiment (3.45 MPa for both of our tests). They were then removed from the pressure vessel and ΔV_q was measured by immersion. Several direct measurements were also taken of sample length and diameter. The samples were returned to the pressure vessel, hydrostatically pressurized to 3.22 MPa (467 psi), and then loaded axially with an additional 0.69 MPa (100 psi) such that $\sigma_1 - \sigma_3$=0.69 MPa and $(\sigma_1 + 2\sigma_3)/3$=3.45 MPa.

The dilatometer/intensifier was then turned on to keep pressure constant and monitor volume change. Additional differences, then, between these experiments and the hydrostatic tests are that the volume of fluid displaced by the loading piston must be included when calculating the time–dependent compaction of the specimen, and the axial load must be regularly updated to keep σ_1 constant.

Cross–sectional area can be measured directly using the LVDT displacement and disk gauges. However, as stated earlier, we were concerned that limited point contact measurements might not constitute a good average estimate for the diameter. We hoped

that a more representative value could be calculated knowing the volume strain, ϵ_v and the axial strain, ϵ_1, which can be calculated from the initial and quasistatic specimen lengths, and the subsequent displacement of the loading piston as indicated by the LVDT. That is,

$$\epsilon_v = \epsilon_1 + \epsilon_2 + \epsilon_3, \tag{1}$$

where

$$\epsilon_v = \frac{\Delta V_q + \Delta V_{dil} + (\Delta L \cdot A)}{V_0}. \tag{2}$$

ΔV_{dil} is the total volume change recorded by the dilatometer during the creep phase, ΔL is the piston displacement indicated by the LVDT (and also the change in specimen length), A is the cross–sectional area of the loading piston, and V_0 is the initial salt volume. The term $(\Delta L \cdot A)$ is the correction factor for the volume of silicone oil displaced by the loading piston as the sample contracts axially. Assuming lateral strain isotropy, that is,

$$\epsilon_2 = \epsilon_3, \tag{3}$$

ϵ_2, ϵ_3, and the current sample diameter and area can be calculated.

For the first of our two prototype experiments, both the dilatometer and the LVDT displacement gauge functioned properly throughout the experiment, and we compare estimates for sample areas using the two methods in Figure 5. Final sample dimensions are not available for comparison with predictions because the the sample was inadvertently compacted axially (and, perhaps, expanded laterally) during a subsequent repressurization to perform a gas permeability measurement. Nevertheless, the areas predicted using the two techniques track quite closely. This result suggests to us that LVDT displacement and disk gauges may be as good a method of measurement as the indirect method of calculating area from piston displacement and dilatometric measurements. Pfeifle [1990] has already reached the same conclusion.

In our second experiment, output from the dilatometer's potentiometer was erratic, registering accelerations in consolidation that were not indicated by the disk gauges or displacement of the loading piston. This erratic behavior was detected only after the test was complete, and data reduction was attempted. Though the presence of a leak was not unequivocally demonstrated, its occurrence was probable. We therefore used disk gauge and axial piston displacement data to estimate both cross–sectional area *and* sample volume, assuming that a right, circular cylindrical shape was maintained. Measurements of the final height of the salt column, along with measurements of the final diameter made at several randomly chosen points along the cylinder's length, are shown in Table 1 along with the predicted values based upon the loading piston's

displacement and disk gauge outputs. Agreement between measured and predicted values is quite good, as are the measured and predicted final volumes for the sample.

2.2.3 Data Acquisition and Reduction

Test data were collected using a computerized data acquisition system. A Hewlett–Packard HP 3497A data acquisition and control unit digitized analog data which were then written to a file on a Hewlett–Packard 9800 series computer. A description of the software is given by D. W. Hannum [unpublished report]. The data were digitized to 0.2 millivolt accuracy over a range from +10 to -10 volts, and written to both a hard disk drive and a printer. Data files were closed frequently and subsequently backed up on 3.5 in–diameter floppies. In the event of a computer failure only the last file on the hard disk would be lost and it could be restored by typing in a few hundred points from the printer hard copy.

Data reduction and analysis were performed on a DEC VAX 8700 using **ANALYSIS**, a data manipulation program developed and maintained by D. J. Holcomb (6232), and **GRAPH II**, a graphics package developed by C. B. Selleck (1411). For both hydrostatic and shear–consolidation experiments, the first step in data reduction was removal of offsets caused by restroking of the intensifier/dilatometers or by test restarts and pressure steps. The second step was to convert transducer data to sample volume changes (ΔV_s), volume strains (ϵ_v), and fractional densities (D). Compressive strains reckoned negative, these quantities are given by

$$\epsilon_v = \frac{\Delta V_s}{V_0} = \left(\frac{\Delta V_{quasi} + \Delta V_{creep}}{V_0} \right) \tag{4}$$

and

$$D = D_0 \left(\frac{1}{1 + \epsilon_v} \right). \tag{5}$$

ΔV_{creep} is the volume change recorded by the dilatometer during the creep phase of the experiment, corrected for loading piston displacement (where necessary).

In addition to basic data manipulation, reduction and plotting, these two programs were used to thin data sets, and take time derivatives. Derivatives of fractional density with respect to time were calculated from data sets thinned from several thousand data points to only a few hundred points. Secant derivatives were then calculated over moving five–point intervals.

In general, agreement between the final volume changes as determined using the (1) direct immersion method and (2) inferred from dilatometric measurements agreed within a few percent (Table 2). We have adjusted the curves presented in the following sections to correspond to the final volume measurement. This has been done by adjusting the value for the quasistatic volume change upward or downward, as necessary. Intermediate fractional densities are shown on the plot when such measurements were made, typically at pressure steps.

3 Test Results and Discussion

3.1 Hydrostatic Compaction Experiments

Conditions and results for the five completed experiments on brine–saturated crushed salt are summarized in Tables 2 and 3. Individual fractional density–time plots for the experiments are given in Figures 6–10, and a summary plot is given in Figure 11. A few remarks are necessary before we summarize the results and compare them to the unsaturated experiments of Holcomb and Shields [1987]. Several of the tests (**09JU88**, **08MR89**, **18AP89**) were run at successively higher pressures: however, only one of these multistage experiments, **09JU88**, was not disrupted by hydraulic system leaks in its later stages. Though we tabulate final fractional densities attained during the higher–pressure stages (Table 3), no curves are presented for stages during which leaks occurred. Our first experiment, **24JL71**, was unintentionally run at a higher pressure; failure of a control unit resulted in overpressuring from 1.72 to 5.31 MPa (770 psi) without either an interim volume measurement or preconditioning at the higher pressure. Nevertheless, the volume change was fully recorded by the dilatometer, and so results are presented for both "stages" (Figure 6). Finally, experiment **18AP89** slowly leaked brine through the basal endplug, directly out of the sample assembly and onto the laboratory floor; it is unknown how this affected the test results.

The summary plot (Figure 11) makes it clear that the current data set contains several inconsistencies which can only be resolved by further testing. The two tests run at 3.45 MPa during their initial stage are closely comparable. However, the test run at 1.72 MPa (**24JL71**) is also very similar to the two 3.45 MPa tests, and, in fact, eventually surpasses the densification rates for the higher pressure experiments.

Furthermore, the two experiments at 6.90 MPa are widely disparate, one compacting more rapidly than the 3.45 MPa tests, as expected, and the other compacting much more slowly; the more slowly–compacting experiment **18AP89** was the test which leaked brine. The possibility cannot be entirely excluded that loss of brine somehow affected the outcome of this experiment; however, it seems improbable that this, alone,

can explain the difference in results. The sample would still be expected to retain some moisture and consolidate more rapidly than the 3.45 MPa experiments on unsaturated crushed salt done by Holcomb and Shields [1987]; in fact, it consolidates much more slowly, as can be seen by comparing a plot of densification rate *vs.* fractional density for **18AP89** (Fig. 18) with similar curves for Holcomb and Shields's [1987] experiments at 3.45 MPa (Fig. 20).

There are several possible explanations for these discrepancies, but none are testable with the current data set and test specimens. First, it is probable that for both unsaturated and brine–saturated specimens, densification occurs by some form of solution–reprecipitation creep (*e.g.*, Shor *et al.* [1981]; Raj [1982]; Spiers and Schutjens [1990]). Details of models for such a mechanism differ, but it is generally agreed that densification rates are proportional to d^{-1} or d^{-3}, where d is the grain size. Though we have taken some steps to ensure that particle size distributions are comparable from specimen to specimen, we have not *guaranteed* that this is the case. Because the predicted inverse dependence on particle size is quite strong, even minor sample–to–sample variations in distribution can have a pronounced effect on densification rate. Differing particle size distributions could also affect the brine distribution and the ability of brine to escape from the specimen. Finally, the possibility exists that proportions of secondary phases (anhydrite, clay minerals) differ from specimen to specimen, and such variations could affect both the densification mechanisms (*e.g.*, Hickman and Evans [in press]) *and* escape of brine from the specimens. Though potential explanations exist for the inconsistencies in our data set, we cannot test these hypotheses in hindsight. It is possible that post–test microstructural studies can shed some light on the problem, but this cannot be relied upon; only further testing more carefully controlled conditions, can clarify or explain these variations.

At this time, because plausible explanations exist for the wide discrepancies in our results, we have no basis on which to exclude any experiment from consideration. However, we show below that it is likely that even our most slowly–consolidating specimen would have continued to densify at geotechnically significant rates and attained a high ($D \geq 0.95$) fractional density at stresses below lithostatic at the WIPP ($\approx$15 MPa).

In Figures 12 and 13 we compare our fractional density–time data for brine–saturated specimens to results for experiments done by Holcomb and Shields [1987] at comparable pressures on unsaturated specimens. For both the 1.72 and 3.45 MPa experiments, our results fall close to, but, nevertheless, distinctly below those of Holcomb and Shields [1987]. Despite the lower consolidation rates, however, the plots make it clear that high fractional densities are attainable for saturated or near–saturated crushed salt specimens, even at pressures well below lithostatic at the WIPP. In particular, experiments **20SE89** and **09JU88** reached fractional densities in excess of 0.95 of intact salt, and

showed no signs of slowing down even at test termination.

A more quantitative way to compare our data with those of Holcomb and Shields [1987] is to compare densification rates at comparable fractional densities; because the contact areas between particles change continuously as densification occurs, comparison of rates between experiments done at constant stress is only valid at constant density [Zeuch, 1989a]. In Figures 14–16 we compare results for our 1.72 and 3.45 MPa experiments with representative experiments from Holcomb and Shields [1987]. At higher fractional densities ($D \geq 0.80$), the unsaturated specimens consolidate at rates between 2.5 and 6 times faster than the saturated samples, confirming that effects related to saturation (*viz.*, isolation of brine–filled pores, reduction in drainage and increase in pore pressure) do slow consolidation rates. Interestingly, however, $\log\left(\frac{dD}{dt}\right)$ continues to decay only linearly with increasing fractional density. Simple extrapolation of these plots would suggest that consolidation could continue at geotechnically significant rates ($\frac{dD}{dt} > 1 \times 10^{-10}$ s^{-1}) right up to full density; such simple extrapolation is risky, however.

Plots of densification rate *vs.* fractional density for experiments done at 6.90 MPa are given in Figures 15 (stage two of **09JU88**) and 17–18 (**18AP89** and **20SE89**, respectively). Holcomb and Shields [1987] did no experiments at these pressures so no results are available for direct comparison with ours. However, these plots allow quantitative comparisons among our own experiments.

Unlike virtually all of our other experiments, **20SE89** (Figure 18) does not show a log–linear decay of densification rate with fractional density; rather, the densification rate begins to level off at $D \approx 0.85$. The reason for this is not known. For fractional densities below about 0.82, **20SE89** consolidates at rates closely comparable to those for **18AP89** during its 6.90 MPa stage (*cf.* Figure 17); had **20SE89**'s rate not leveled off, it would have looked much like the sluggishly–consolidating **18AP89** at higher fractional densities. However, though **09JU88** was compacted both at 3.45 and 6.90 MPa, its fractional density range during the latter phase overlaps that of **20SE89**; thus, densification rates for the two experiments can be validly compared within the overlapping range. Within that fractional density range ($0.91 \leq D \leq 0.95$), the densification rates are virtually identical (compare Figures 15 and 18). The close similarity of rates for **09JU88** and **20SE89** at 6.90 MPa, and the previously–noted disparate behavior of **18AP89** as compared to the other four experiments (Figure 11) suggests to us that the results for **20SE89** and **09JU88** are more representative of behavior at 6.90 MPa. It is interesting to note, however, that even if **18AP89**'s log–linear decay of rate with fractional density continued unabated during the 6.90 MPa stage, the sample would still have continued to consolidate at a geotechnically significant rate up to a fractional density of about 0.95.

Our results suggest the following tentative conclusions: (1) Effects associated with brine–saturation do retard consolidation rates to some extent; for experiments done at comparable pressures (1.72 and 3.45 MPa), unsaturated specimens compact 2.5 to 6 times faster. It must be remembered, however, that the estimated error in our final measured values for D is ± 0.02, and was probably comparable in the study by Holcomb and Shields [1987]. Examination of Figures 14, 15 and 16 indicates that the measured differences between our results and those of Holcomb and Shields [1987] may not be significant within the resolution of our fractional density measurements. (2) Despite the (possibly) lower consolidation rates for brine–saturated, crushed salt samples, fractional densities in excess of 0.95 are attainable on laboratory time scales at pressures well below lithostatic at the WIPP.

3.2 Shear–Consolidation Experiments

A cautionary note is in order before discussing the results of our shear–consolidation experiments. Both tests were prototypes, and both experienced problems. As described below, we believe that the results for **12OC89** are quite credible despite these problems. However, unresolved difficulties remain regarding **08MY89**, and extensive interpretation was involved in the data reduction. We present the results only because so few data are available, and because we believe we have been cautious in our interpretations. However, it must be remembered that our results are, at best, rough estimates of the effects of shear stress on consolidation. We now comment on the problems encountered and the assumptions made in interpreting our data.

What should have been an obvious error in the measurement of starting components for experiment **08MY89** was detected only after (1) the test was terminated and a final volume measurement made, (2) the sample had been inadvertently compacted by an unknown amount during pressurization following reinsertion into the pressure vessel, and (3) the specimen was disassembled. As discussed above, the volume of the non–salt components is essential in calculating salt volumes and fractional densities throughout the course of the experiment. To calculate the starting volume of the salt, we have used the value for the volume of the non–salt components for experiment **12OC89** on the assumption that the volume of these parts should not vary much from test to test. This is borne out by examination of the test set–up sheets and logs for hydrostatic compaction experiments. The starting volume for the salt, so estimated, agrees within 16 cm^3 of the value calculated from initial direct measurements on the assembled specimen. We have estimated the final fractional density, 0.92, from measurements on cores extracted from the sample and machined into right circular cylinders after the sample was slightly crushed; therefore, these measurements may overestimate the final

fractional density. However, after assuming the value for the volume of the starting components as outlined above, recalculation of the volume as determined by immersion yields a result identical to the final fractional density determined from the weights and dimensions obtained from the cores.

Owing to the uncontrolled compaction of the specimen, however, the value of 0.92 probably should be regarded only as an upper bound. Calculations of volume changes and fractional densities based on axial and lateral LVDT measurements agree closely with the results calculated from the dilatometer, D=0.88. The good agreement between indirect dilatometric, and direct volume measurements (from averaged diameter and length measurements) suggests, therefore, that the final fractional density for **08MY89** could have been as low as 0.88 and that the higher value is indeed the result of crushing. We have adjusted the fractional density–time plot to correspond to the higher value determined by immersion for comparison in Fig. 19 with results of the hydrostatic experiments of Holcomb and Shields [1987], done at 3.45 MPa. Were the data adjusted to correspond to the lower value, the curve would shift downward and would fall roughly in the middle of Holcomb and Shields's [1987] results at 3.45 MPa (Figs. 19 and 20). Results from this test suggest, at best, only a slightly faster rate of consolidation than the experiments by Holcomb and Shields [1987], and possibly, no detectable effect at all.

As noted above, the dilatometer failed during **12OC89** and the volume was calculated using disk gauge data and the axial LVDTs only. However, as shown in Table 1, direct, post–test measurements of sample length and diameter agree very well with values calculated indirectly from the gauge outputs. We therefore believe that these results are credible.

Volume and density measurements for our two prototype shear–consolidation experiments, **08MY89** and **12OC89**, are summarized in Tables 4 and 5. Plots of mean stress, axial stress and stress difference *vs.* time may be found in Appendix A, Figures A1–A3 and A4–A6. **12OC89** experienced several interruptions, and, during (roughly) the last half of the experiment was run at a stress difference of about 1.38 MPa (200 psi) and a mean stress of 3.68 MPa (533 psi) (Figures A4 and A5). Fractional density–time plots for the two experiments are given in Figure 19; as can be seen in the figure, these small departures from the specified conditions had minimal effects on the consolidation behavior of **12OC89**. Also shown in Figure 19, for comparison with our data, are the results from Holcomb and Shields's [1987] 3.45 MPa experiments.

At this time we have no explanation for the wide disparity in our two results, though we note that experiment **08MY89** attained a somewhat higher quasistatic fractional density than did **12OC89** (0.72 *vs.* 0.67; Table 4). **08MY89** agrees much more

closely with Holcomb and Shields's [1987] 3.45 MPa experiments, which also exhibited relatively high quasistatic fractional densities ranging from 0.72 to 0.77 (*cf.* Holcomb and Shields [1987], Table 2). Though this observation serves to confirm our belief that early–time behavior has a strong influence on subsequent consolidation [Holcomb and Zeuch, 1987; 1990], the reason remains unclear.

In Figure 20, plots of densification rate *vs.* fractional density are given for the same experiments shown in Figure 19. Results for **08MY89** agree well with those of Holcomb and Shields [1987], while those for **12OC89** fall somewhat outside the scatter of the earlier experiments. At higher fractional densities (D>0.80), densification rates for a "representative" experiment from Holcomb and Shields [1987] data set are about one decade faster than those for **12OC89**, though their most slowly–consolidating specimen exhibited rates only about 2.5 times faster.

In summary, the results for our two prototype shear–consolidation experiments are disparate, and further testing will be required to resolve the discrepancy. Data for **08MY89** suggest that small shear stresses have no deleterious effect on consolidation rates, and may actually slightly accelerate densification. Results for **12OC89** suggest that addition of a small shear stress may slightly retard consolidation rates, though by at most an order of magnitude.

4 Summary and Conclusions

As part of an ongoing experimental program, we have completed five hydrostatic compression experiments on brine–saturated, crushed rock salt from the WIPP site. The purpose of the experiments is to evaluate the effects, if any, of brine–saturation on densification rates and terminal fractional densities. The experiments were done at 20±0.5°C, pressures of 1.72, 3.45, 6.90 or 10.34 MPa, and were run for up to eleven months in duration. Results to date indicate that effects related to brine–saturation do indeed have a retarding effect on densification rates; unsaturated specimens [Holcomb and Shields, 1987] consolidate at rates 2.5 to 6 times faster than saturated specimens at the same pressures. However, fractional densities in excess of 0.95 are nevertheless attainable in the laboratory at pressures below lithostatic at the WIPP site. The retarding effect is presumably caused by the entrapment of brine within the specimens as the connected porosity "pinches off" and pores become isolated; this results in a reduction in drainage of the specimens and an increase in pore pressure which resists further compaction.

We have also completed two prototype shear–consolidation experiments on moist, but unsaturated, crushed WIPP salt. The objective of these and other experiments planned

for the future, is to evaluate the effects of small shear stresses on densification rates. The experiments were done at 20±0.5°C, a mean stress of 3.45 MPa, and a stress difference of 0.69 MPa. Results for the two experiments were disparate, and further experimentation will be necessary to resolve the discrepancy. Comparison with hydrostatic compaction experiments run at 3.45 MPa [Holcomb and Shields, 1987] suggests that, at worst, a small shear stress may retard consolidation rates by about an order of magnitude. However, it is possible that further testing will show that shear stress actually has an accelerating effect on densification rates.

Extensive experimental studies are planned for the future, both at Sandia [Wawersik, 1988; Zeuch, 1989b] and at contractor–owned laboratory facilities [Brodsky, 1990]. It is expected that the planned test matrices will resolve the discrepancies noted in this report. Experiments planned for the future include a number of tests in which particle size will be carefully controlled in order to investigate the mechanism(s) that operate during consolidation [Wawersik, 1988]. Microstructural studies will be performed on the resulting specimens. As mentioned above, it is probable that some form of fluid–phase enhanced creep is responsible for densification, but details of the process are unclear. Shor *et al.* [1981] found densification rates for brine–saturated, fine–grained (75 to 420 micrometres) crushed salt to be proportional to d^{-3}, and interpreted their data in terms of an early sintering model proposed by Coble. In this model, the densification rate is controlled by the rate of diffusion of Na^{+1} and Cl^{-1} through the brine. However, the pressing experiments performed by Shor *et al.* [1981] were done in a piston–die assembly and die friction effects cast serious doubts on their results (*e.g.*, Zeuch [1989a; 1990]). Raj [1982] found densification rates for relatively coarse–grained (200–3000 micrometres) halite to be proportional to d^{-1} under a uniaxial stress of 2.85 MPa, and concluded that the densification rate was interface–controlled, that is, controlled by the rate of solution of NaCl into the brine. However, Raj's [1982] experiments were also performed in a piston–die apparatus; Spiers and Schutjens [1990] further suggest that Raj apparently obtained his relationship between densification rate and grain size from pseudo–steady–state values of $\left(\frac{dD}{dt}\right)$, rather than comparing rates at constant fractional density. If this is true, then Raj's results are even more doubtful.

Spiers and Schutjens [1990] performed hydrostatic compaction experiments on relatively fine–grained (180–355 micrometres) brine–saturated halite aggregates. At pressures below 2.15 MPa, Spiers and Schutjens found densification rates to be proportional to d^{-3}, indicating diffusion–controlled densification; microstructural observations provided "classical evidence... that densification was caused predominantly by 'pressure solution'... ." Above 2.15 MPa, densification occurred by a combination of increased plasticity and minor fluid–assisted recrystallization. Our existing and planned experiments span a much broader range of stresses and pressures than those of Spiers and Schutjens [1990], and it will be interesting to compare our microstructures of Spiers and

Schutjens. We have examined thin sections of one unsaturated specimen compacted at 1.72 MPa [Holcomb and Shields, 1987; Exp# **20AU51**] and observed extensive, not minor, recrystallization. This result differs from that of Spiers and Schutjens [1990], who apparently detected no recrystallization at such low pressures. The reason for the discrepancy is unknown, but may relate to the longer time span of Holcomb and Shields' experiments (19 days for **20AU51**), differing particle size distributions or differing compositions. This suggests that, at least for coarser particle sizes and phases representative of material likely to be used as backfill at the WIPP or other waste isolation facilities sited in bedded or domal salt formations, mechanisms other than, or in addition to, classical pressure solution, may play an important role. We plan to investigate this possibility in the future.

5 References

Bosworth, W. (1981). *Strain-induced preferential dissolution of halite.* Tectonophysics, **78**:509–525.

Brodsky, N.S. (1990). *Activity Plan for Hydrostatic and Shear Consolidation Tests on WIPP Crushed Salt.* Draft Activity Plan RSI/AP–018, rev. 0, RE/SPEC, Inc., Rapid City, SD.

Heard, H.C., and F.J. Ryerson (1986). *Effect of cation impurities on steady-state flow of salt.* In: Hobbs, B.E., and H.C. Heard, eds., *Mineral and Rock Deformation: Laboratory Studies*, Geophys. Mono. v.36, American Geophysical Union, Washington, D.C., pp.99–115.

Hickman, S.H., and B. Evans (in press). *Experimental pressure solution in halite, 1: the effect of grain/interphase boundary structure.* J. Geol. Soc. London.

Holcomb, D.J., and D.W. Hannum (1982). *Consolidation of Crushed Salt Backfill Under Conditions Appropriate to the WIPP Facility.* Rept. No. SAND82–0630, Sandia National Laboratories, Albuquerque, NM.

Holcomb, D. J., and M. J. McNamee (1984). *A displacement gage for the rock mechanics laboratory.* Exp. Mech., **26**:217–223.

Holcomb, D.J., and M.E. Shields (1987). *Hydrostatic Creep of Crushed Salt With Added Water.* Rept. No. SAND87–1990, Sandia National Laboratories, Albuquerque, NM.

Holcomb, D.J., and D.H. Zeuch (1988). *Consolidation of Crushed Rock Salt, Part I: Experimental Results for Dry Salt Analyzed Using a Hot-Pressing Model.* Rept. No. SAND88–1469, Sandia National Laboratories, Albuquerque, NM.

Holcomb, D.J., and D.H. Zeuch (1990). *Modeling the consolidation of a porous aggregate of salt as isostatic hot-pressing.* J. Geophys. Res., **95**:15,611–15,622.

Johnson, J. N., and S. J. Green (1976). *The mechanical response of porous media subject to static loads.* In: Cowin, S. C., and M. M. Carroll (Editors) *The Effects of Voids on Material Deformation*, The American Society of Mechanical Engineers, New York City, pp. 93–123.

Kingery, W.D., J.M. Woulbroun and F.R. Charvat (1963). *Effect of applied pressure on densification during sintering in the presence of a liquid phase.* J. Amer. Ceram. Soc., **46**:391–395.

Nowak, E.J., D.F. McTigue and R. Beraun (1988). *Brine Inflow to WIPP Disposal Rooms: Data, Modeling, and Assessment.* Rept. No. SAND88–0112, Sandia National Laboratories, Albuquerque, NM.

Pfeifle, T.W. (1990). *Consolidation, Permeability and Strength of Crushed Salt/Bentonite with Application to the WIPP.* Rept. No. SAND90–7009, Sandia National Laboratories, Albuquerque, NM.

Schuler, K. W. (1979). *Lateral-deformation gage for rock-mechanics testing.* Exp. Mech., **18**:477–480.

Shor, A.J., C.F. Baes, Jr., and C.M. Canonico (1981). *Consolidation and Permeability of Salt in Brine.* Rept. No. ORNL–5774, Oak Ridge National Laboratory, Oak Ridge, TN.

Sjaardema, G.D., and R.D. Krieg (1987). *A Constitutive Model for the Consolidation of WIPP Salt and its Use in Analyses of Backfilled Shaft and Drift Configurations.* Rept. No. SAND87–1977, Sandia National Laboratories, Albuquerque, NM.

Spiers, C.J., and P. M. T. M. Schutjens (1990). *Densification of crystalline aggregates by fluid-phase diffusional creep.* In: Barber, D.J. and P.G. Meredith (eds.), *Deformation Processes in Minerals, Ceramics and Rocks*, Unwin Hyman, London, pp.334–353.

Stein, C.L. (1985). *Mineralogy in the Waste Isolation Pilot Plant (WIPP) Facility Stratigraphic Horizon.* Rept. No. SAND85–0321, Sandia National Laboratories, Albuquerque, NM.

Wawersik, W.R. (1988). *Five-Year Plan for WIPP and 6232 Support.* Internal memorandum to L.D. Tyler, 6332, April 8, 1988. Sandia National Laboratories, Albuquerque, NM.

Wawersik, W.R., and D.H. Zeuch (1986). *Modeling and mechanistic interpretation of creep of rock salt below 200 °C.* Tectonophysics **121**:125–152.

Zeuch, D.H. (1989a). *Isostatic Hot-Pressing Mechanism Maps for Pure and Natural Sodium Chloride: Applications to Nuclear Waste Isolation in Bedded and Domal Salt Formations.* Rept. No. SAND88–2207, Sandia National Laboratories, Albuquerque, NM.

Zeuch, D.H. (1989b). *Proposed FY90 Laboratory Testing on Crushed Salt in Support of the WIPP Plugging and Sealing Program.* Internal memorandum to E.J. Nowak, 6346, November 2, 1989. Sandia National Laboratories, Albuquerque, NM.

Zeuch, D.H. (1990). *Isostatic hot-pressing mechanism maps for pure and natural sodium chloride: applications to nuclear waste isolation in bedded and domal salt formations.* Int. J. Rock Mech. Min. Sci. & Geomech. Abstr., **27**:505–524.

6 Tables

Table 1: Comparison of Direct Final Diametral and Axial Specimen Dimensions with Values Predicted from Disk Gauge and LVDT Measurements on Specimen **12OC89**

Average of eight direct, diametral measurements on sample:	8.06 cm
Value determined from average of data from two disk gauges:	8.10 cm
Average of two direct measurements of sample length:	11.1 cm
Sample length determined from axial piston displacement:	11.2 cm
Sample volume calculated from averaged point contact measurements:	566.6 cm^3
Sample volume measured by the immersion method:	582.7 cm^3
Ratio of measured to calculated sample volume:	0.97

Table 2: Summary of Volume Measurements for Hydrostatic Experiments

Test ID	Stage (MPa)	Mass (g)	V_0 (cc) (immersion)	V_f (cc) (immersion)	ΔV_q (cc) (immersion)	ΔV_c (cc) (immersion)	ΔV_c (cc) (dilatometer)	ΔV_f (cc) (immersion)	$\frac{\Delta V_{c(immer)}}{\Delta V_{c(dilat)}}$
24JL71	1.72 & 5.31	1722.6	1282.5	854.8	-109.8	-318.0	-297.5	-427.7	1.07
09JU88	3.45	1696.7	1243.3	872.2	-110.4	-260.7	-265.3	-371.1	0.98
09JU88-2	6.90	1696.7	872.2	834.1	-2.3	-35.9	-37.1	-38.1	0.97
08MR89	3.45	1705.0	1258.9	864.2	-136.0	-258.7	-279.3	-394.7	0.93
08MR89-2	10.34	1705.0	864.2	861.0	0.0	-3.3	N/A	-3.2	N/A
20SE89	6.90	1632.6	1276.9	799.0	-219.9	-258.0	-267.9	-477.9	0.96
18AP89	6.90	1652.1	1290.3	872.5	-223.4	-194.4	-207.7	-417.8	0.94
18AP89-2	10.34	1652.1	872.5	848.9	-8.5	-15.1	N/A	-23.6	N/A

Test ID : Test name

Stage: Pressure stage of the test

Mass: Mass of the salt (grams) used in the experiment.

V_0 (immersion): Starting volume of the salt, determined by the immersion method.

V_f (immersion): Final volume of the salt, determined by immersion method.

ΔV_q (immersion): Quasistatic volume change of salt, measured by immersion method.

ΔV_c (immersion): Time-dependent volume change of salt, measured by the immersion method.

ΔV_c (dilatometer): Time-dependent volume change of salt, measured by the dilatometer.

ΔV_f (dilatometer): Total volume change of salt, measured by the immersion method.

Table 3: Summary of Density and Saturation Measurements for Hydrostatic Experiments

Test ID	Stage (MPa)	D_0	D_q	D_f (calculated)	D_f (measured)	Void Space (cc)	H_2O Added (cc)	% Sat.	H_2O Expelled (cc)
24JL71	1.72 & 5.31	0.63	0.69	0.92	0.94	367.2	310.9	87	257
09JU88	3.45	0.64	0.70	0.91	0.91	342.1	329.0	96	307
09JU88-2	6.90	0.91	0.91	0.95	0.95	—	—	–	—
08MR89	3.45	0.63	0.71	0.95	0.92	325.6	292.0	90	261
08MR89-2	10.34	0.92	0.92	N/A	0.93	—	—	–	—
20SE89	6.90	0.60	0.72	0.97	0.96	295.0	245.5	83	220
18AP89	6.90	0.60	0.72	0.90	0.88	294.5	264.5	89	N/A
18AP89-2	10.34	0.88	0.89	N/A	0.91	—	—	–	—

Test ID: Test name.

Stage: Pressure stage of test (MPa).

D_0: Starting fractional density determined from volume measurements made by the immersion method.

D_q: Quasistatic fractional density determined from volume measurements made by the immersion method.

D_f (calculated): Final fractional density computed from dilatometric data.

D_f (measured): Final fractional density determined from immersion–method volume measurements.

Void Space: Void space (cc) estimated from direct volume and density measurements.

H_2O Added: Volume of brine (cc) added to the sample.

% Sat.: Estimated percentage of void space filled with brine.

H_2O Expelled: Volume of brine (cc) collected in the graduated cylinder during the experiment.

Table 4: Summary of Volume Measurements for Shear–Consolidation Experiments

Test ID	Mean Stress (MPa)	Mass (g)	V_0 (cc) (immersion)	V_f (cc) (immersion)	ΔV_q (cc) (immersion)	ΔV_c (cc) (immersion)	ΔV_c (cc) (dilatometer)	ΔV_f (cc) (immersion)	$\frac{\Delta V_{c(immer)}}{\Delta V_{c(dilat)}}$
08MY89	3.45	1063.8	772.7	537.8	80.8	154.2	128.0	235.0	1.2
12OC89	3.45	1100.4	862.7	582.7	99.9	180.1	N/A	280.0	N/A

Test ID : Test name

Stage: Pressure stage of the test

Mass: Mass of the salt (grams) used in the experiment,

$\mathbf{V_0}$ **(immersion)**: Starting volume of the salt, determined by the immersion method.

$\mathbf{V_f}$ **(immersion)**: Final volume of the salt, determined by immersion method.

$\mathbf{\Delta V_q}$ **(immersion)**: Quasistatic volume change of salt, measured by immersion method.

$\mathbf{\Delta V_c}$ **(immersion)**: Time–dependent volume change of salt, measured by the immersion method.

$\mathbf{\Delta V_c}$ **(dilatometer)**: Time–dependent volume change of salt, measured by the dilatometer.

$\mathbf{\Delta V_f}$ **(dilatometer)**: Total volume change of salt, measured by the immersion method.

Table 5: Summary of Density Measurements for Shear–Consolidation Experiments

Test ID	Mean Stress (MPa)	D_0	D_q	D_f (calculated)	D_f (measured)	H_2O Added (cc)
08MY88	3.45	0.64	0.72	0.88	0.92	26 cc
12OC89	3.45	0.60	0.67	N/A	0.88	26 cc

Test ID: Test name.

Stage: Mean stress of test (MPa).

$\mathbf{D_0}$: Starting fractional density determined from volume measurements made by the immersion method.

$\mathbf{D_q}$: Quasistatic fractional density determined from volume measurements made by the immersion method.

$\mathbf{D_f}$ **(calculated)**: Final fractional density computed from dilatometric data.

$\mathbf{D_f}$ **(measured)**: Final fractional density determined from immersion–method volume measurements.

$\mathbf{H_2O}$ **Added**: Volume of brine (cc) added to the sample.

7 Figures

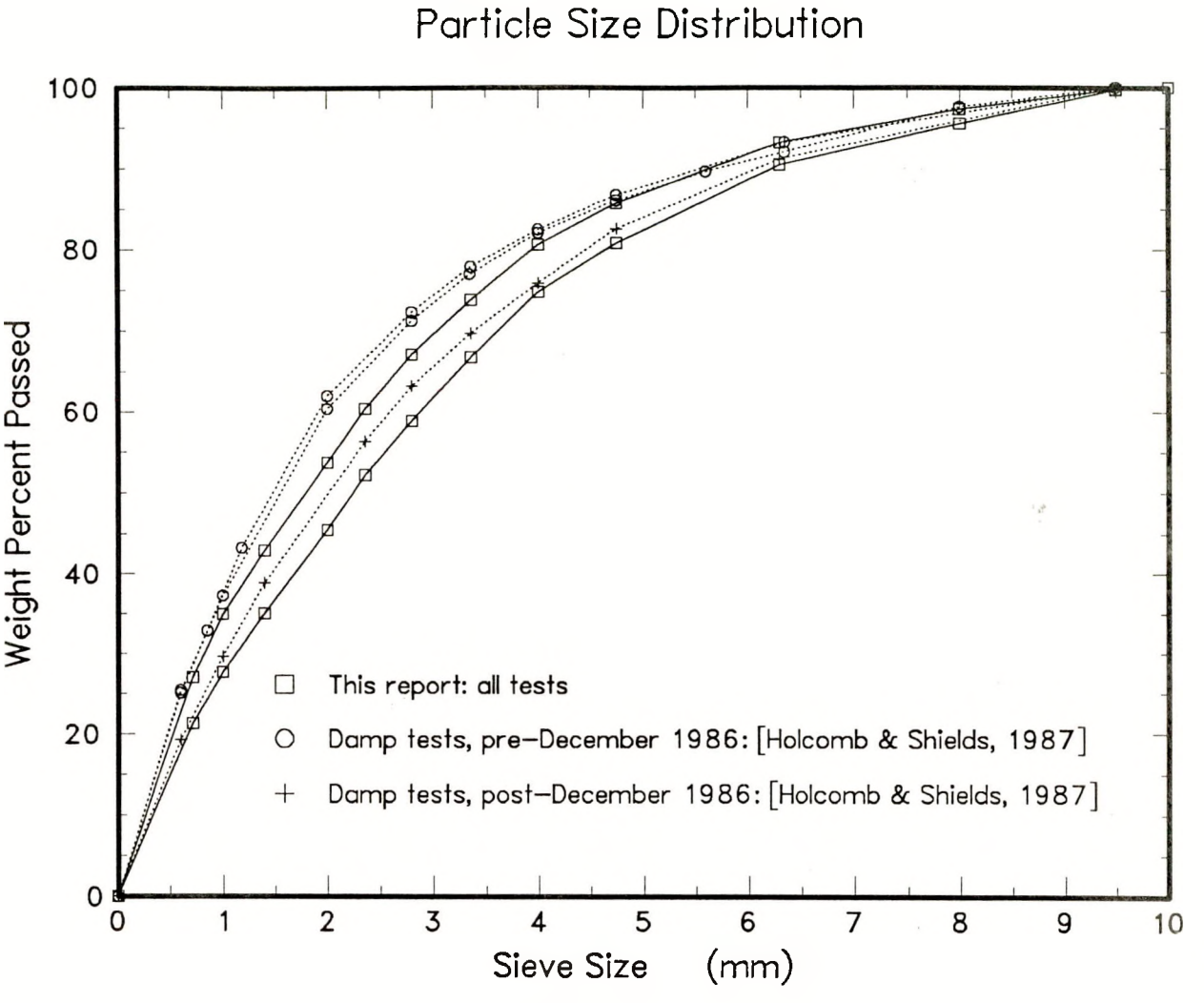

Figure 1: Particle size distribution for the crushed WIPP salt used in this study. Shown for comparison are size distributions for the two crushed salt batches used by Holcomb and Shields [1987]. Our material was drawn from the "post–December 1986" batch, and our results bracket those of Holcomb and Shields.

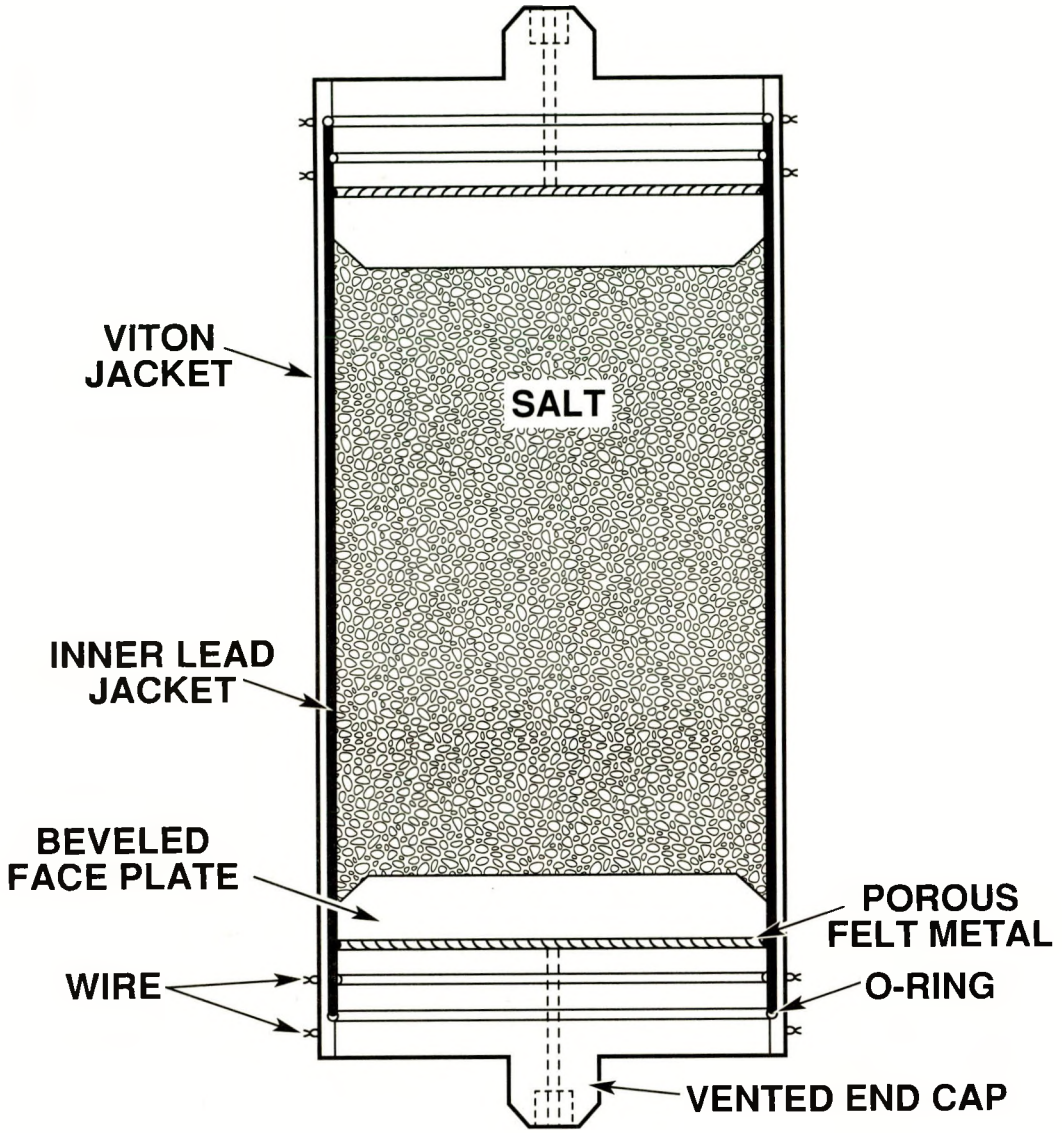

Figure 2: Sample assembly used for crushed salt testing in this study. Two different sizes were used for the hydrostatic and shear–consolidation experiments (see text).

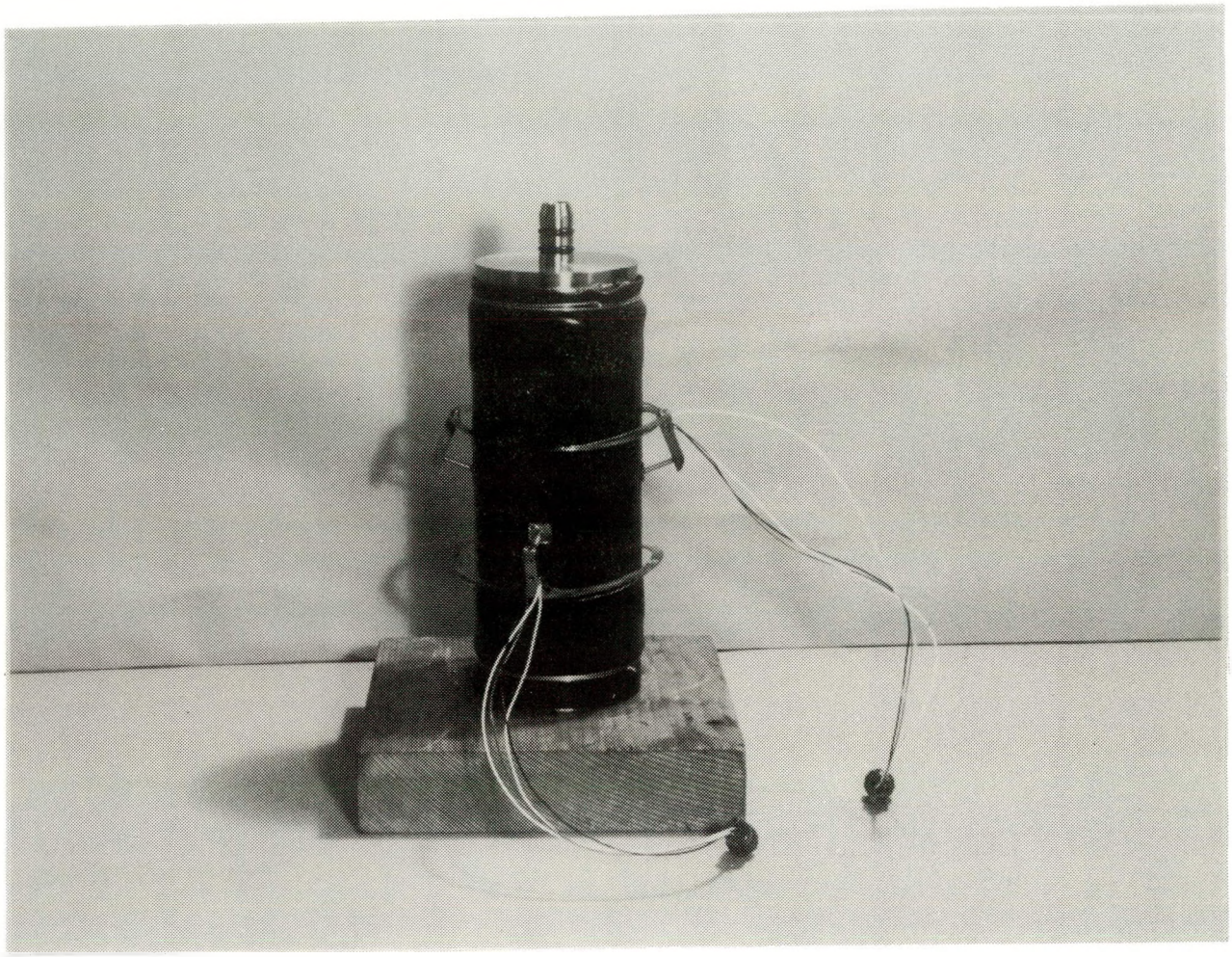

Figure 3: Photograph showing the manner in which disk gauges [Schuler, 1979] are mounted on the outer Viton jacket of the sample assembly. Note that two gauges were mounted across approximately perpendicular diameters.

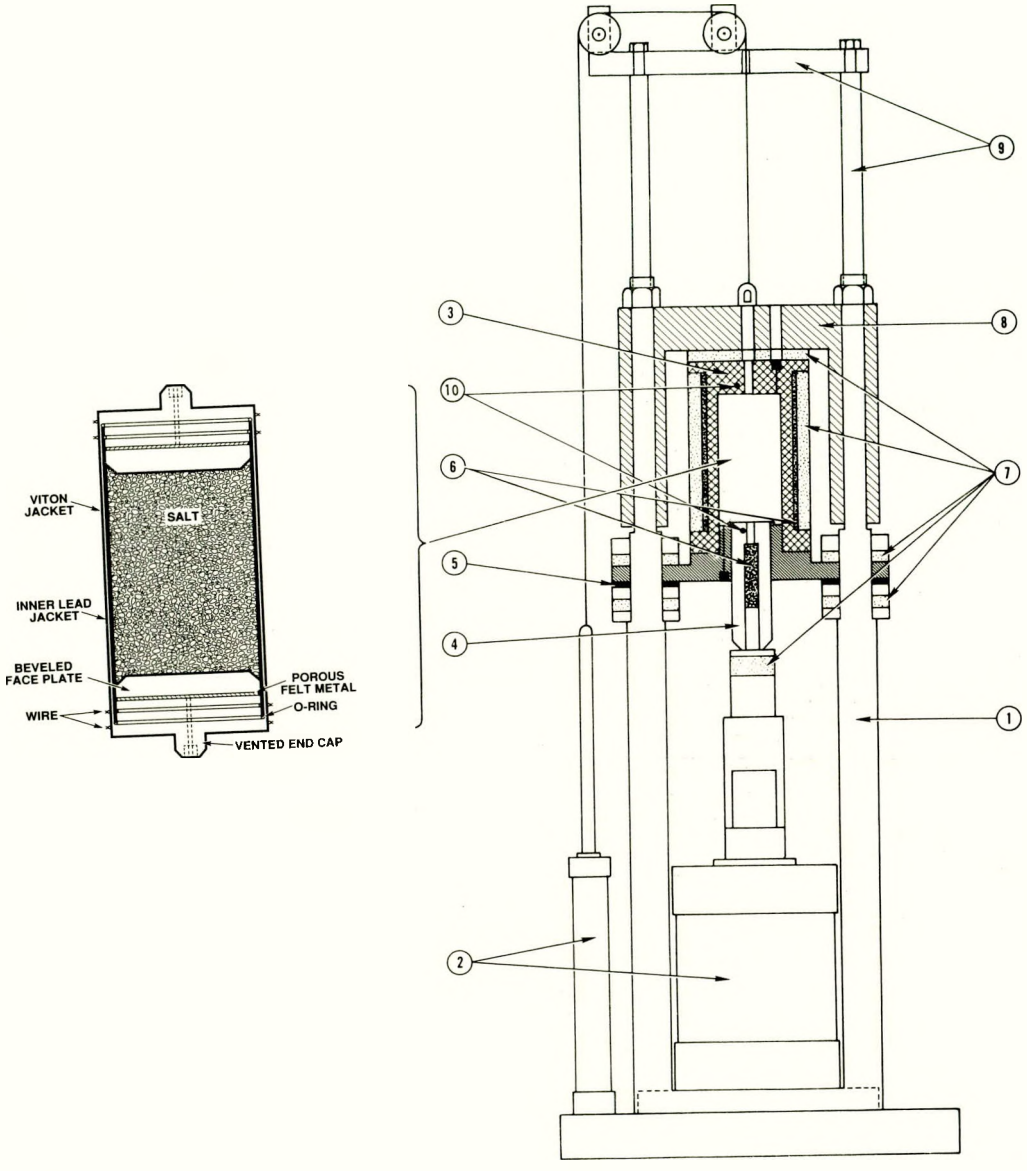

Figure 4: Triaxial testing apparatus designed by W.R. Wawersik and used for our hydrostatic compaction experiments on brine–saturated crushed salt specimens. Numbers on the figure correspond to the following components: (1) tie rods for reaction frame; (2) hydraulic actuators; (3) pressure vessel; (4) deviatoric loading piston; (5) Belleville washers; (6) heaters; (7) insulation; (8) crosshead with guide rods; (9) frame extension/lifting fixture; (10) thermocouple location.

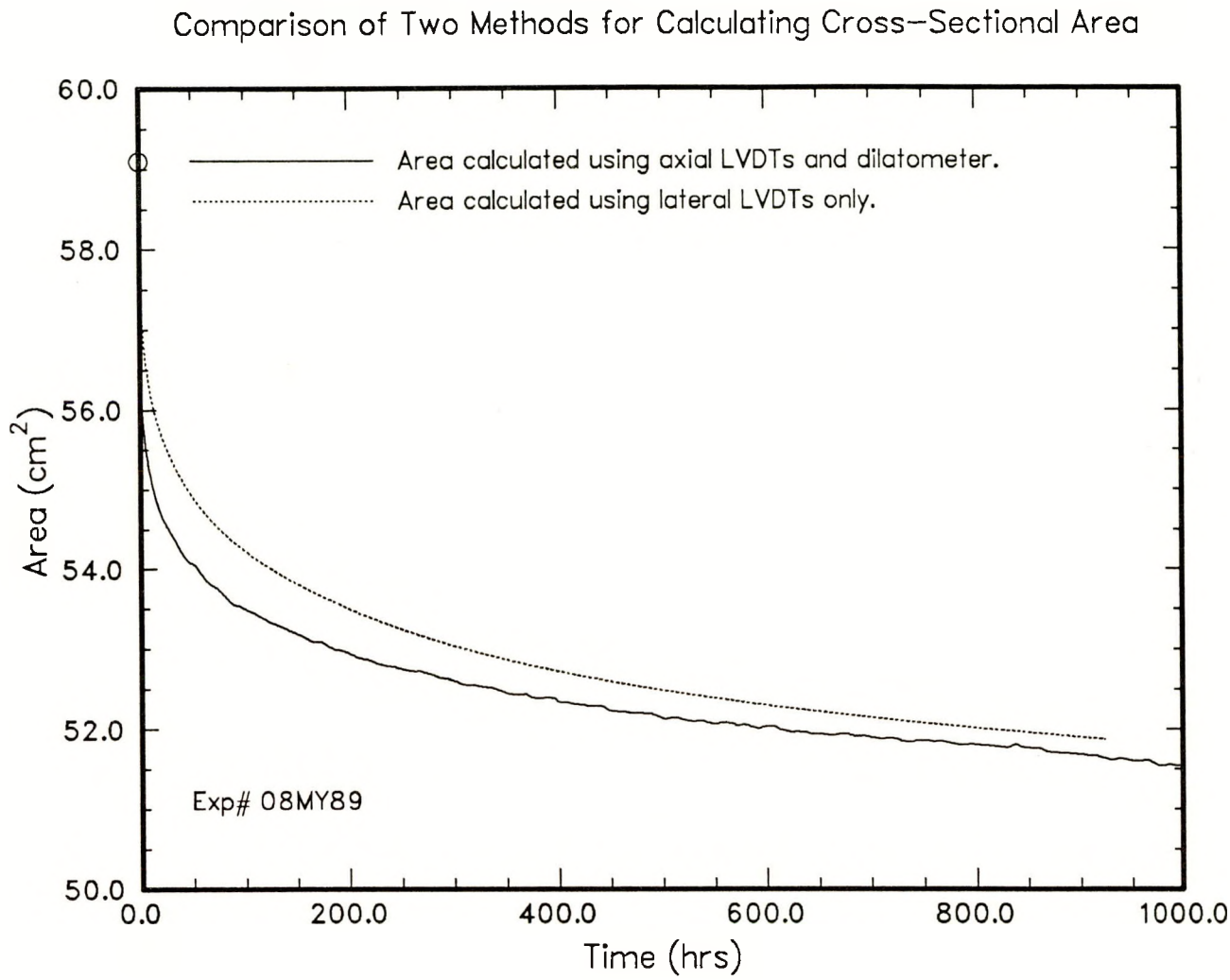

Figure 5: Comparison of two methods for calculating cross–sectional area of the compacting sample. The circle marks the cross–sectional area following quasistatic compaction. The dotted line represents the cross–sectional area calculated from the diametral changes indicated directly by the LVDT displacement gauge [Holcomb and McNamee, 1984]. The solid line represents the cross–sectional area determined from the volumetric strain, ϵ_v, measured by the dilatometer, the axial strain, ϵ_1, measured by the external LVDTs, assuming that the lateral strains are isotropic, *i.e.*, $\epsilon_2 = \epsilon_3$. The lateral strains can then be calculated from Eq. (1) (see text).

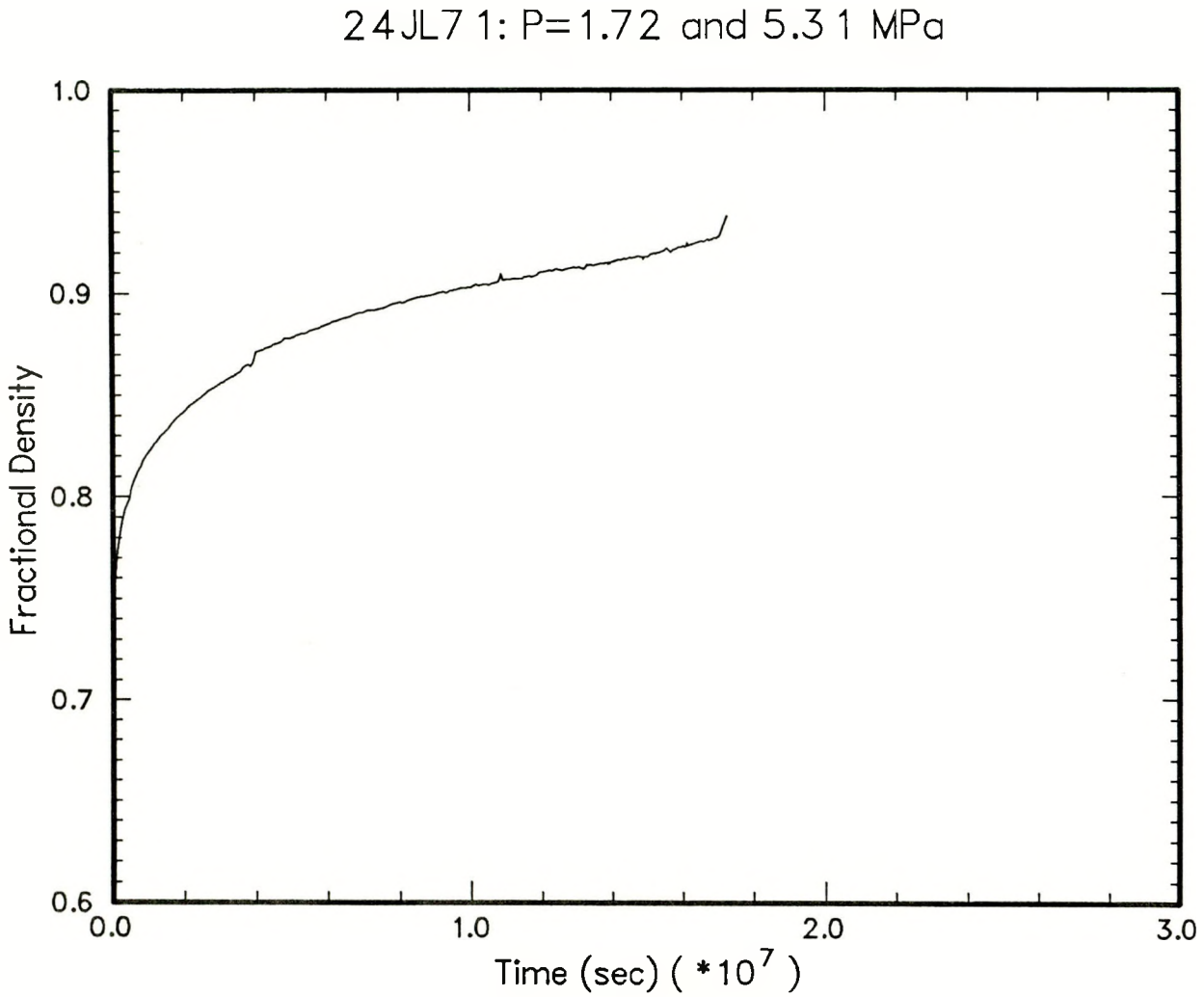

Figure 6: Fractional density–time plot for experiment **24JL71**. The final upturn in the plot is where accidental overloading occurred.

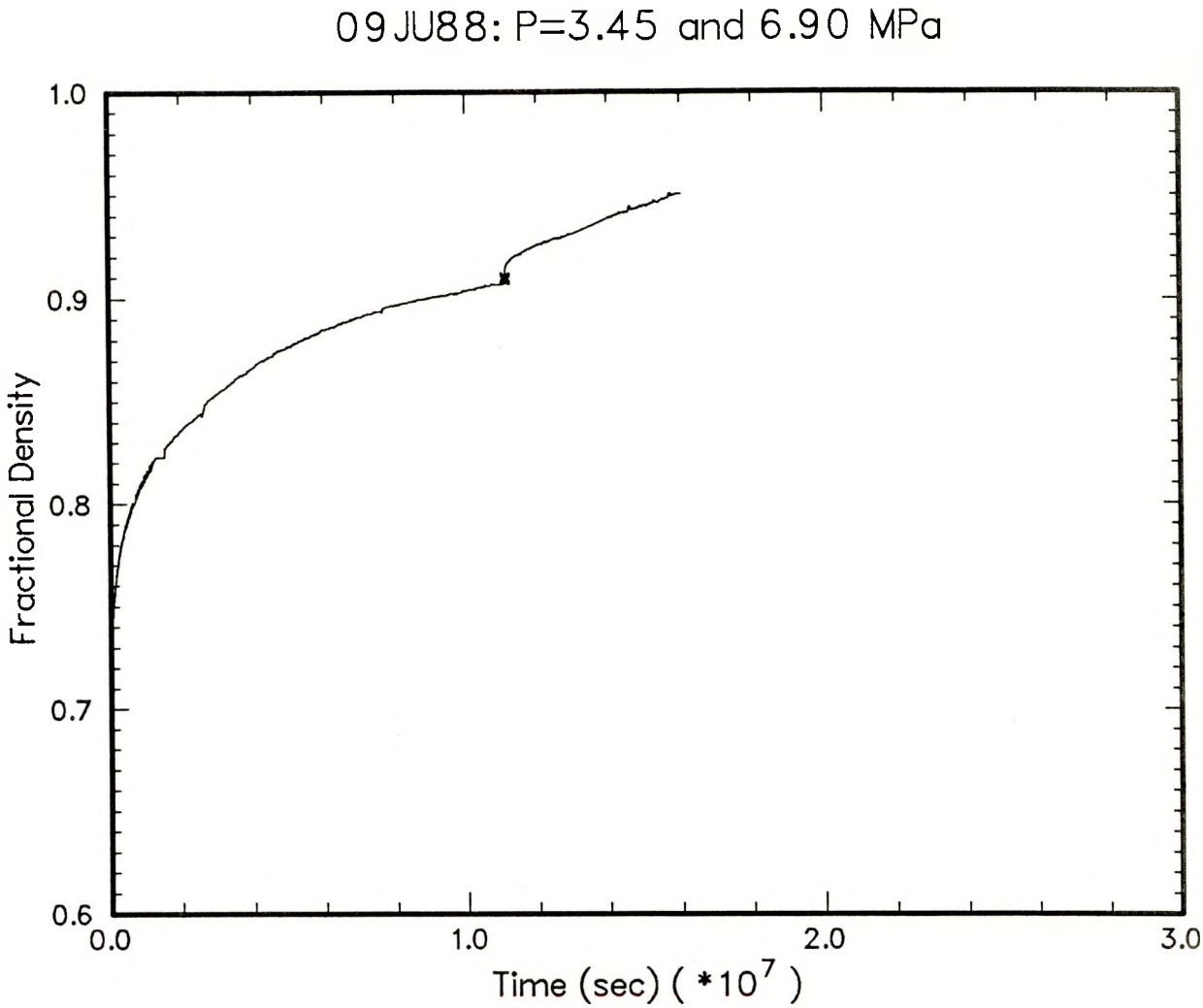

Figure 7: Fractional density–time plot for experiment **09JU88**. The nearly–overlying crosses represent (1) the direct volume measurement at the end of the 3.45 MPa stage and (2) the direct volume measurement following quasistatic conditioning prior to the 6.90 MPa creep stage.

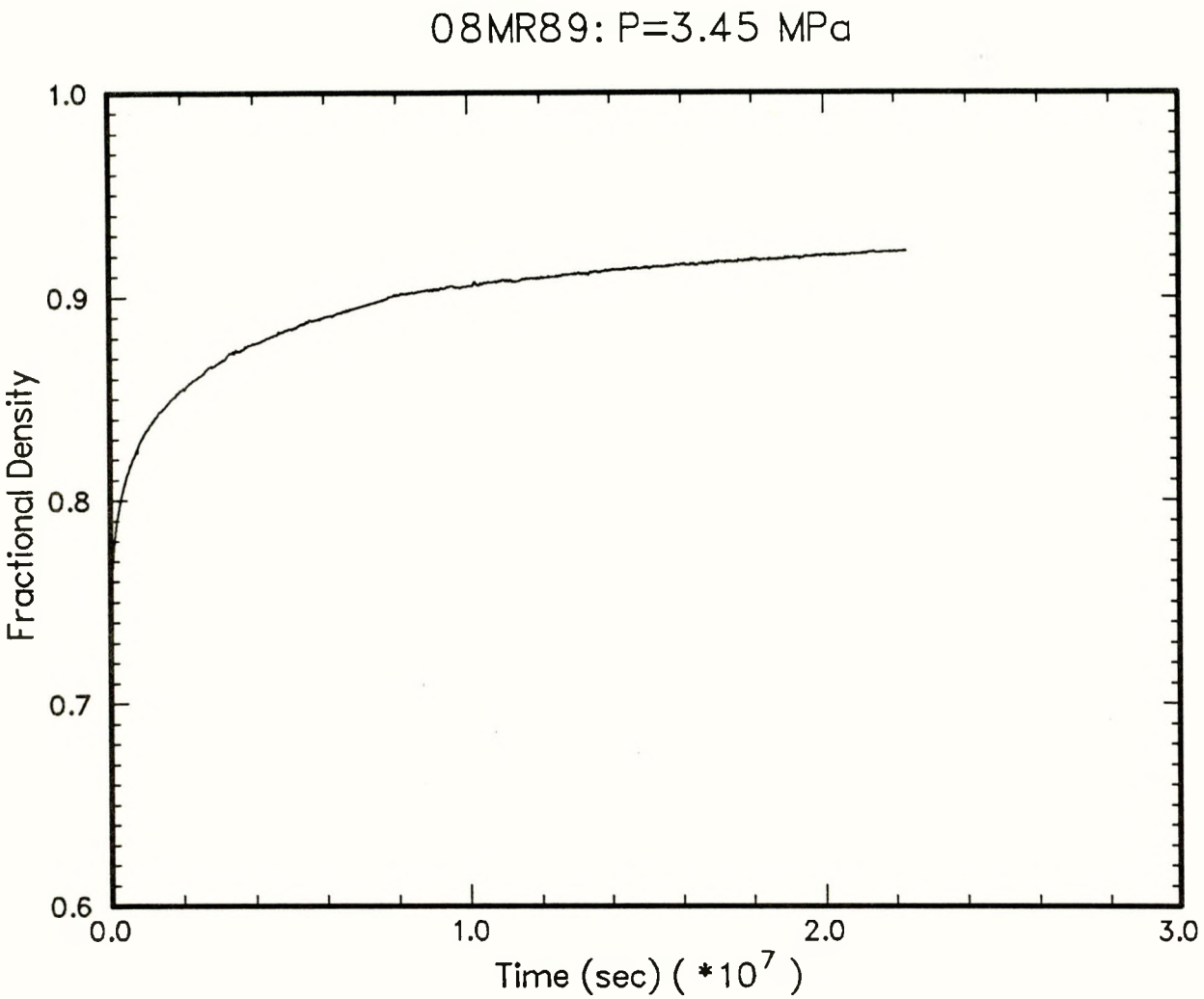

Figure 8: Fractional density–time plot for experiment **08MR89**. A subsequent 10.34 MPa stage was run on this specimen, but leaks made the dilatometric data useless. However, the volume change measured by immersion during this stage, and the final measured fractional density are shown in Tables 2 and 3.

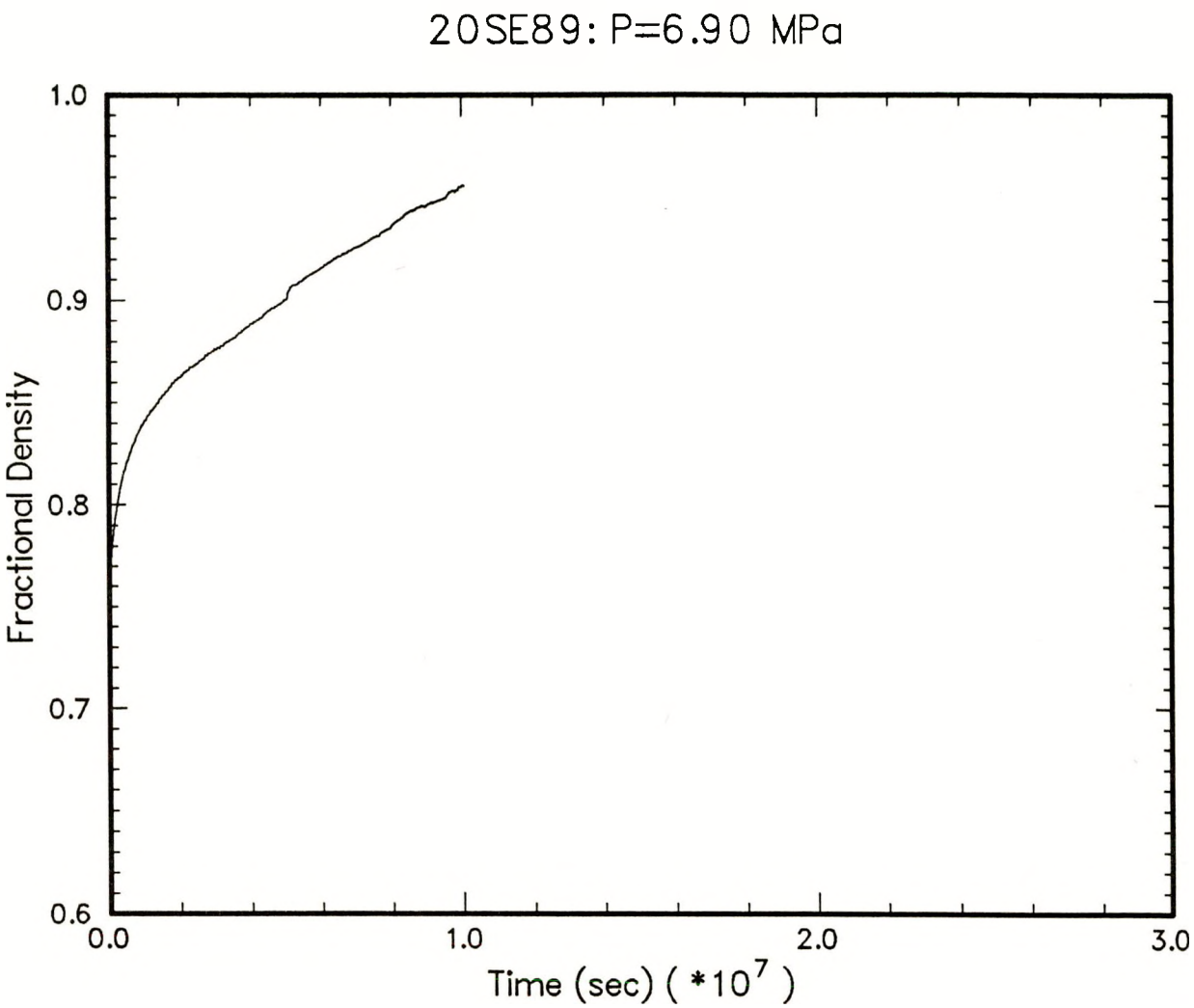

Figure 9: Fractional density–time plot for experiment **20SE89**.

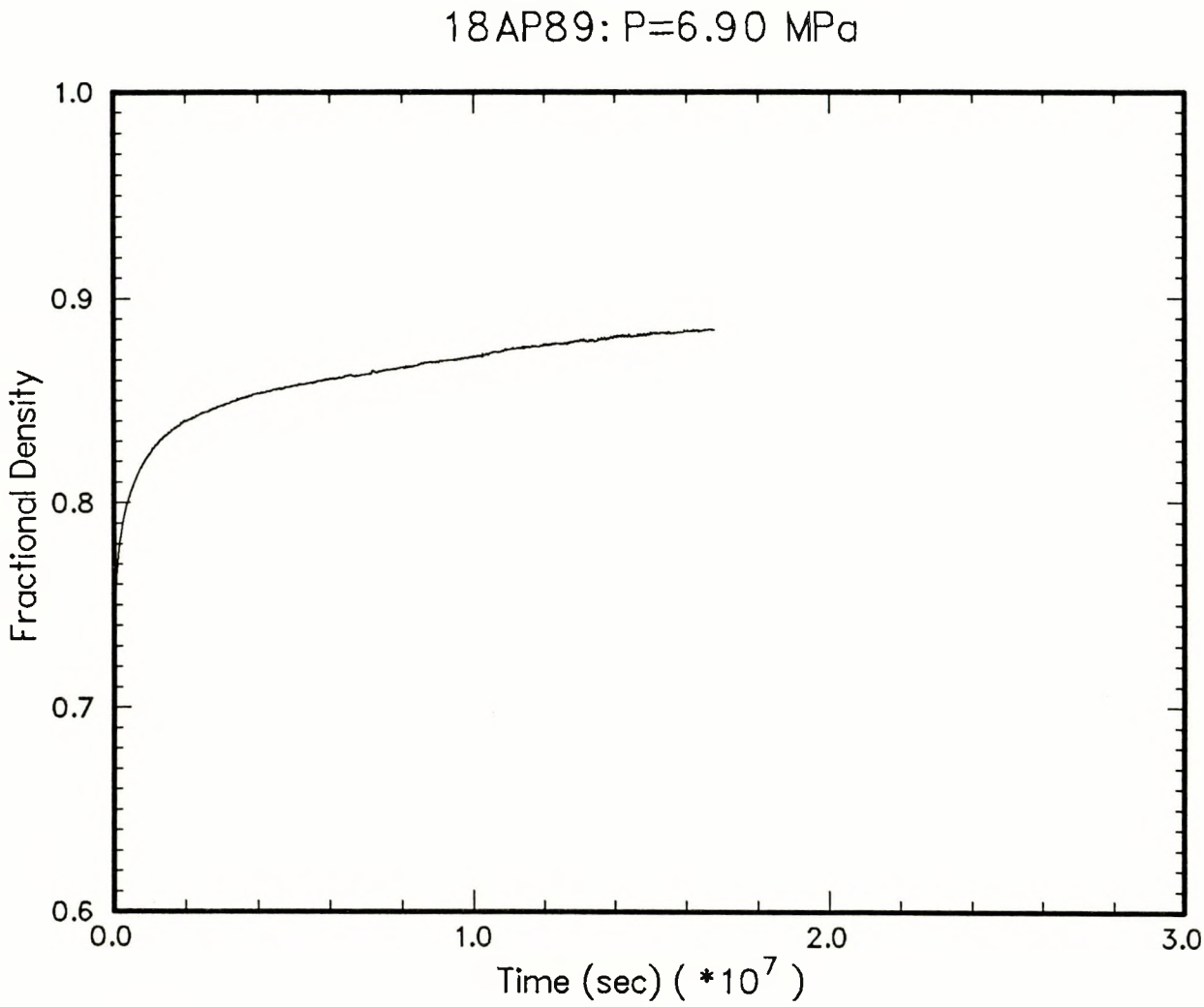

Figure 10: Fractional density–time plot for experiment **18AP89**. An additional stage at 10.34 MPa was run on this sample, but leakage rendered the dilatometric data useless. Measurements made by direct immersion are given in Tables 2 and 3.

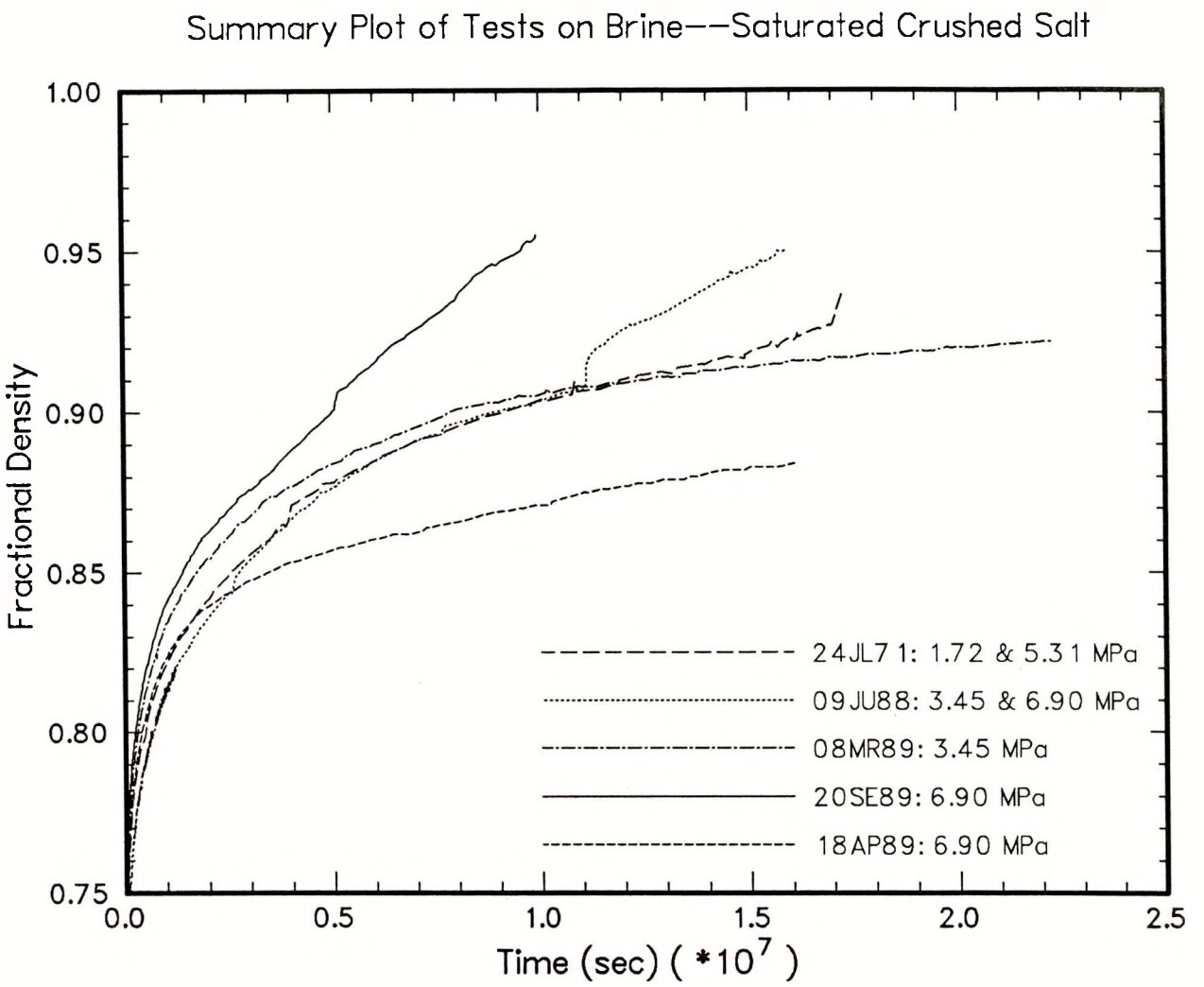

Figure 11: Summary plot of fractional density–time data for hydrostatic compaction experiments on brine–saturated crushed WIPP rock salt. See text for discussion.

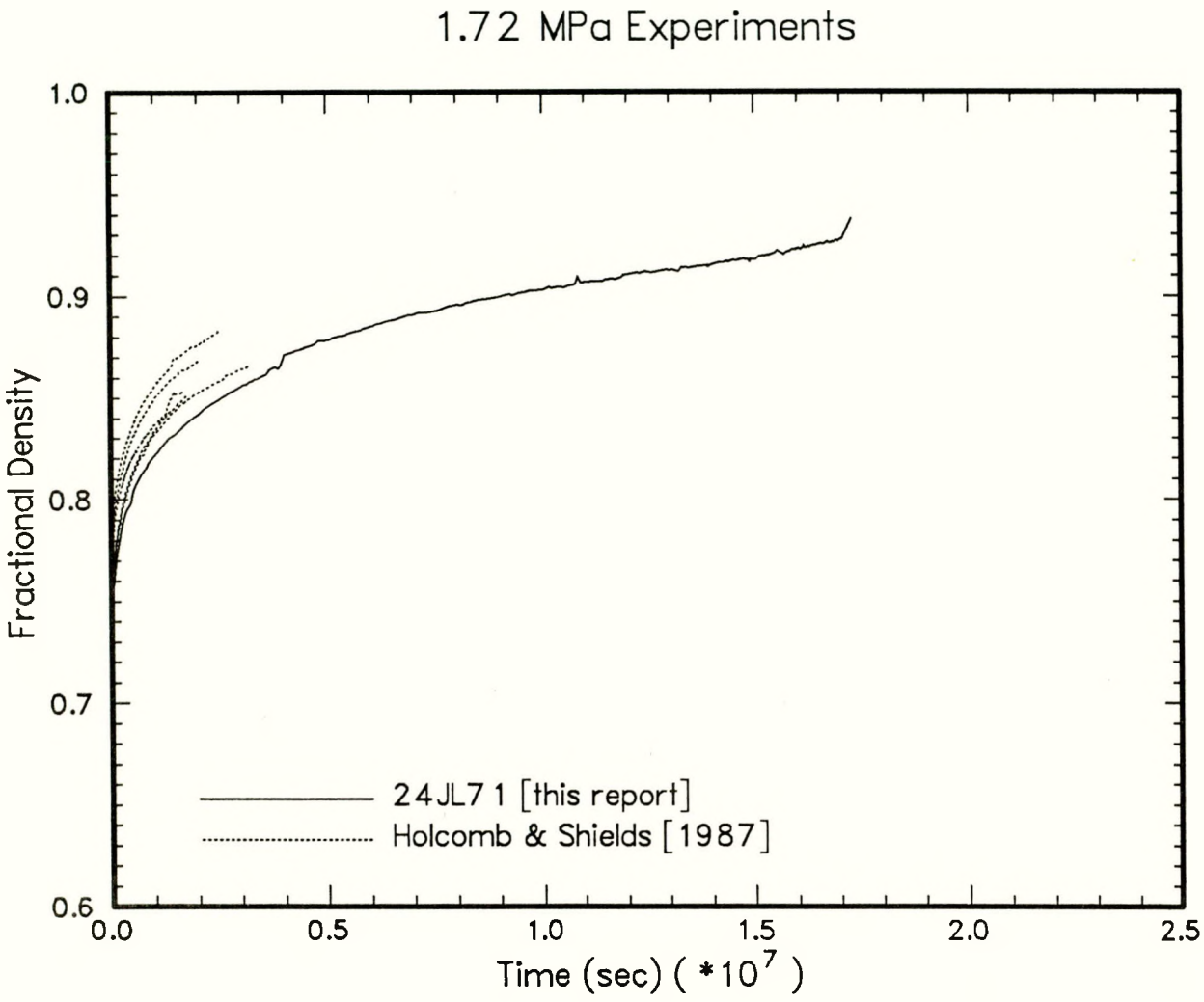

Figure 12: Comparison of experiment **24JL71**, P=1.72 MPa, with tests done by Holcomb and Shields [1987] on unsaturated crushed salt at the same pressure.

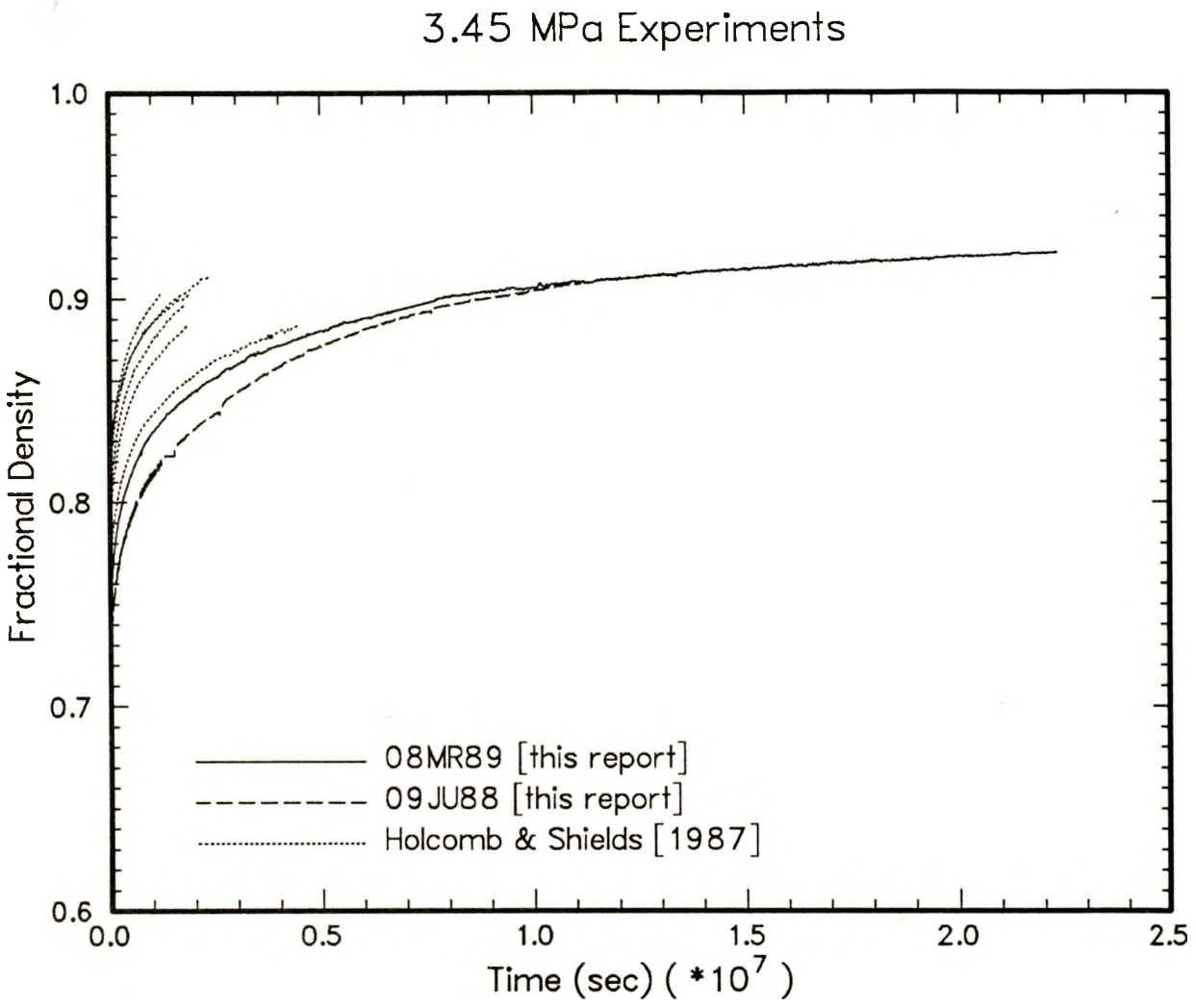

Figure 13: Comparison of experiments **08MR89** and **09JU88**, P=3.45 MPa, with tests done by Holcomb and Shields [1987] on unsaturated crushed salt at the same pressure.

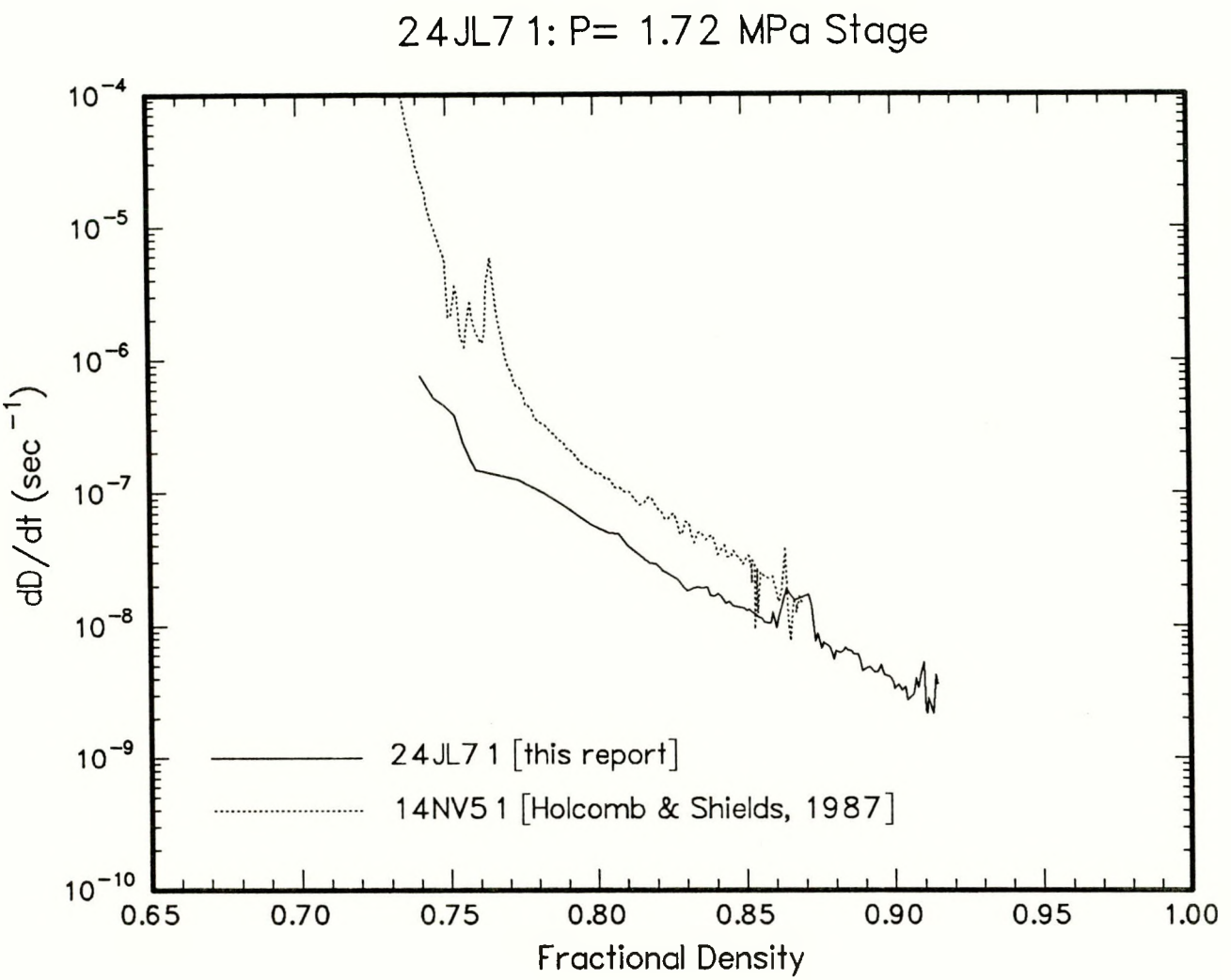

Figure 14: Plot of time derivative of fractional density *versus* fractional density for experiment **24JL71** (solid line). Shown for comparison are data from a representative experiment on unsaturated crushed salt done by Holcomb and Shields [1987] (**14NV51**) at the same pressure, 1.72 MPa.

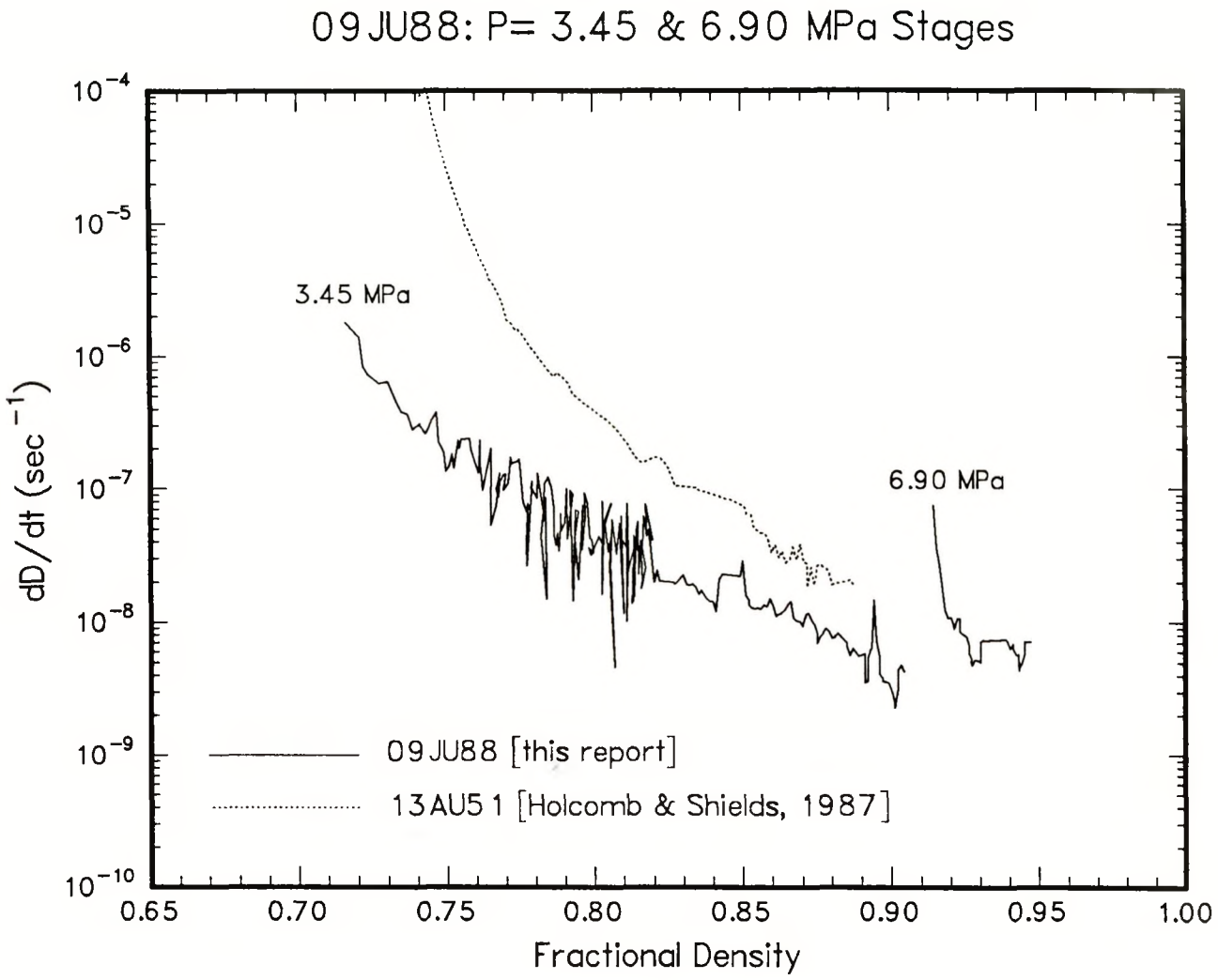

Figure 15: Plot of time derivative of fractional density *versus* fractional density for experiment **09JU88** (solid lines). The break in the solid line represents the change in pressure from 3.45 to 6.90 MPa. Shown for comparison with the 3.45 MPa stage are data from a representative experiment on unsaturated crushed salt done by Holcomb and Shields [1987] at 3.45 MPa (their experiment **13AU51**).

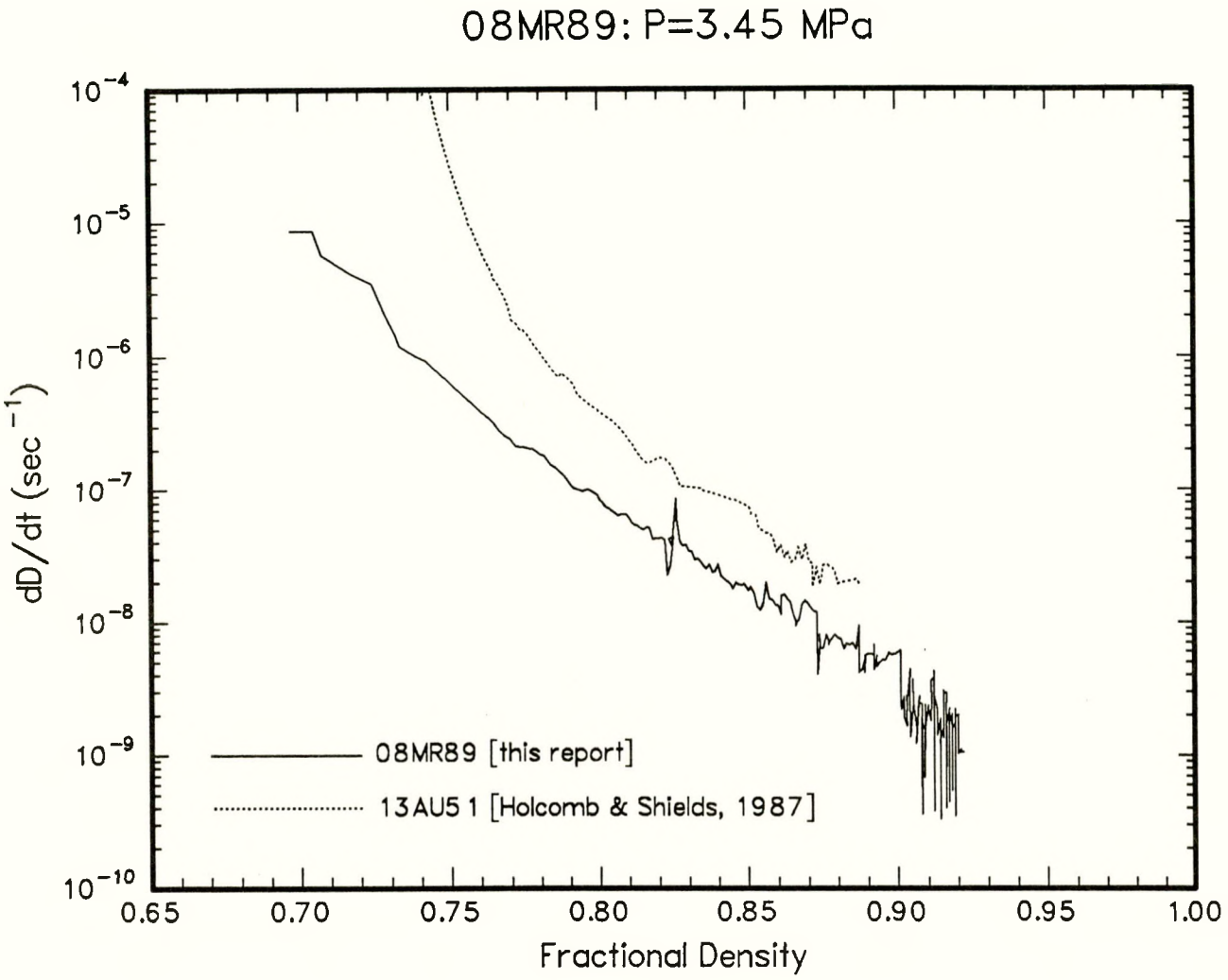

Figure 16: Plot of time derivative of fractional density *versus* fractional density for experiment **08MR89** (solid line). Shown for comparison are data from a representative experiment on unsaturated crushed salt done by Holcomb and Shields [1987] (**13AU51**) at the same pressure, 3.45 MPa.

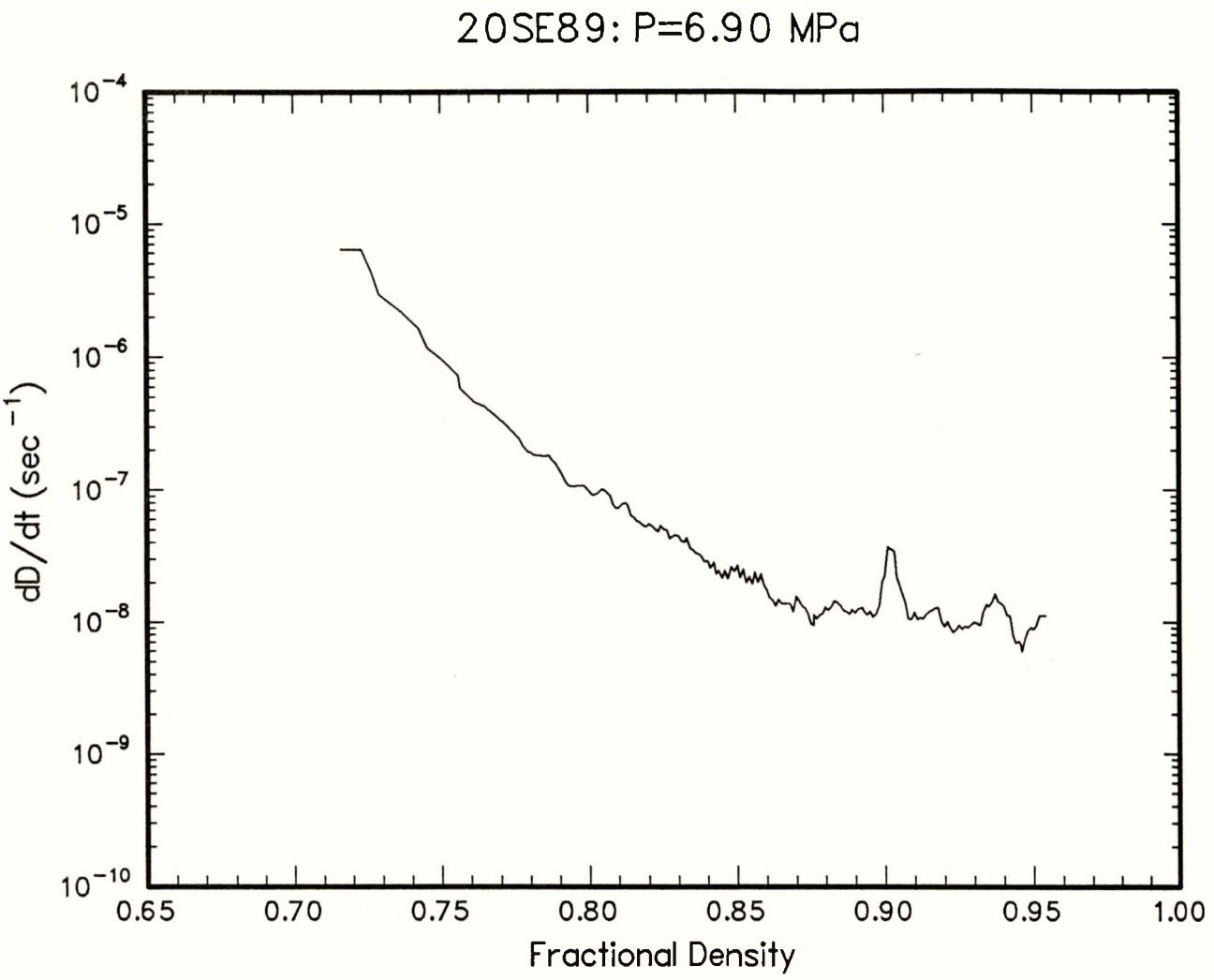

Figure 17: Plot of time derivative of fractional density *versus* fractional density for experiment **20SE89**.

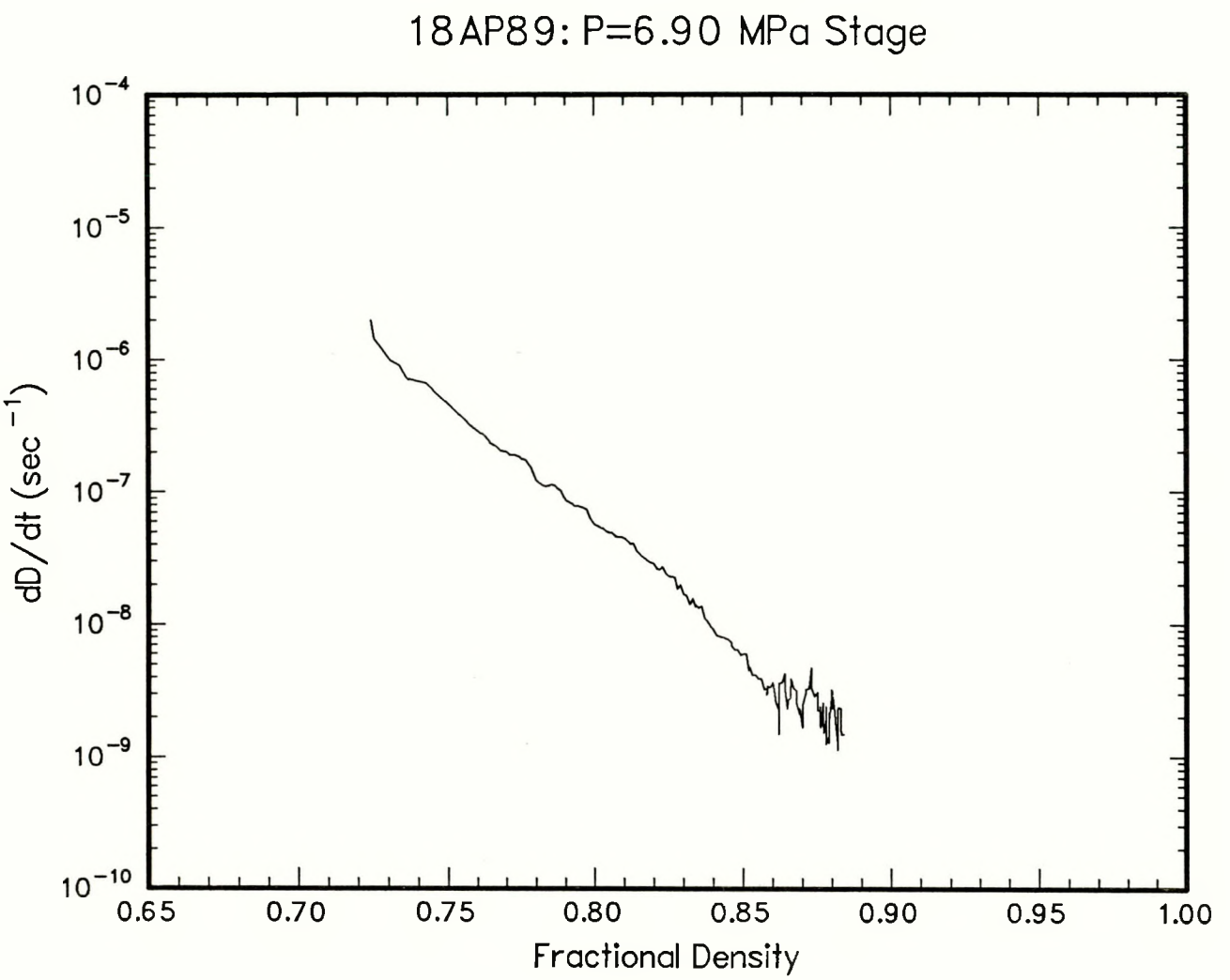

Figure 18: Plot of time derivative of fractional density *versus* fractional density for experiment **18AP89**.

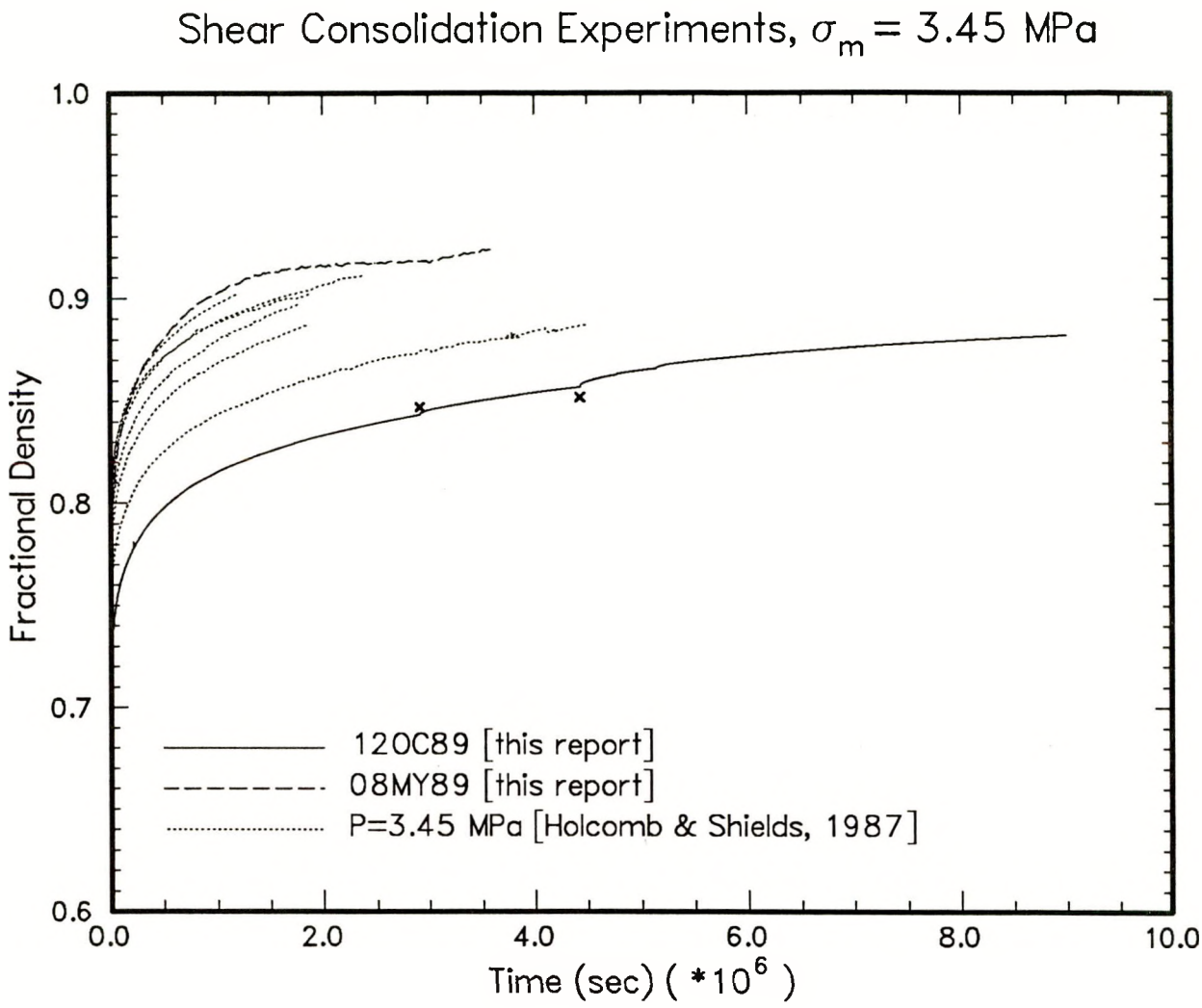

Figure 19: Plots of fractional density *versus* time for our two shear–consolidation experiments, **08MY89** and **12OC89**, the dashed and solid lines, respectively. The crosses located along the solid line represent fractional densities determined from direct volume measurements by the immersion method during interruptions in the experiment. Shown for comparison are results from all of the experiments performed by Holcomb and Shields [1987] at 3.45 MPa on unsaturated, crushed WIPP salt (dotted lines).

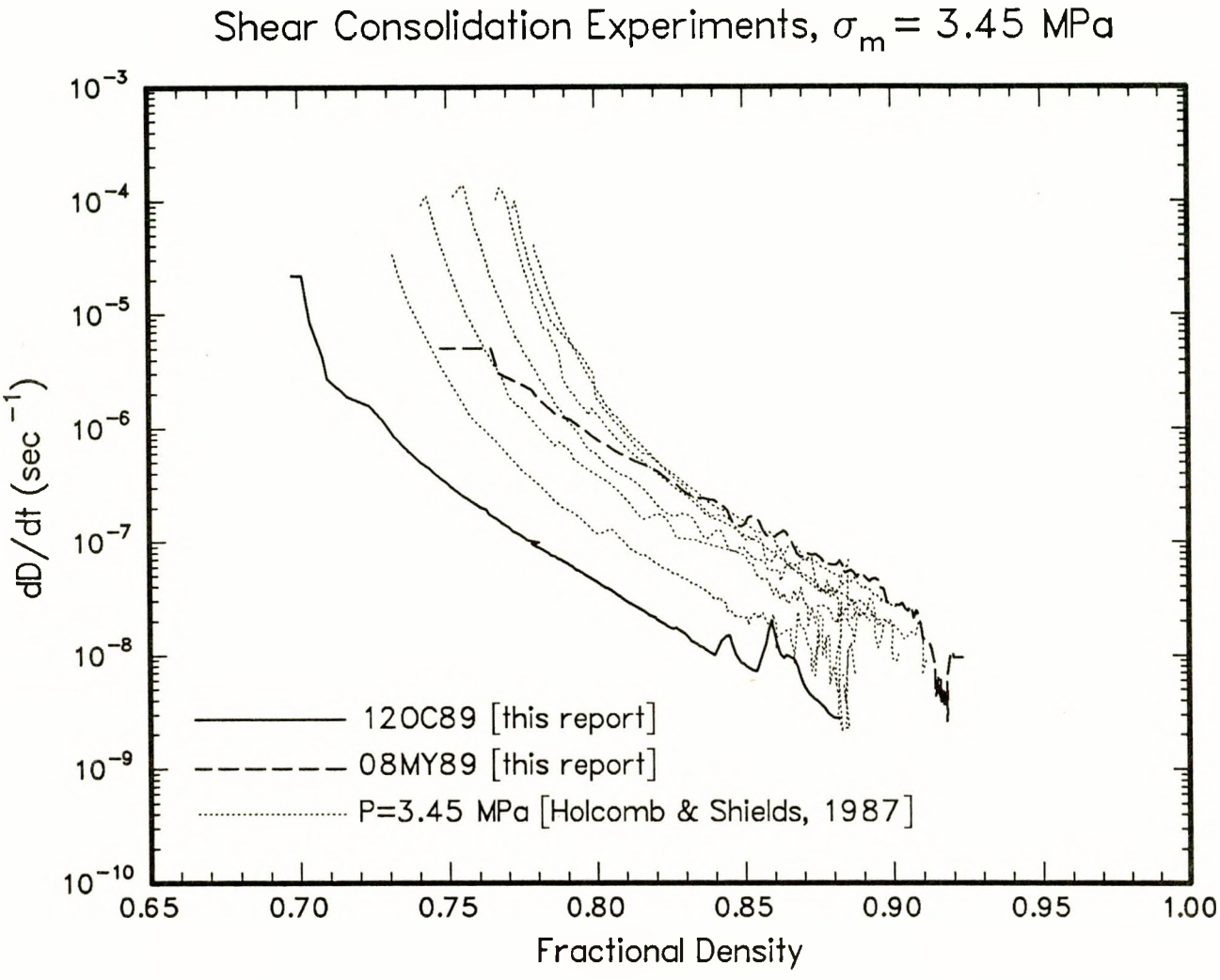

Figure 20: Plot of the time derivative of fractional density *versus* fractional density for our two shear–consolidation experiments, **08MY89** and **12OC89**, the dashed and solid lines, respectively. Shown for comparison are results from all of the experiments performed by Holcomb and Shields [1987] at 3.45 MPa on unsaturated, crushed WIPP salt (dotted lines).

8 Appendix A

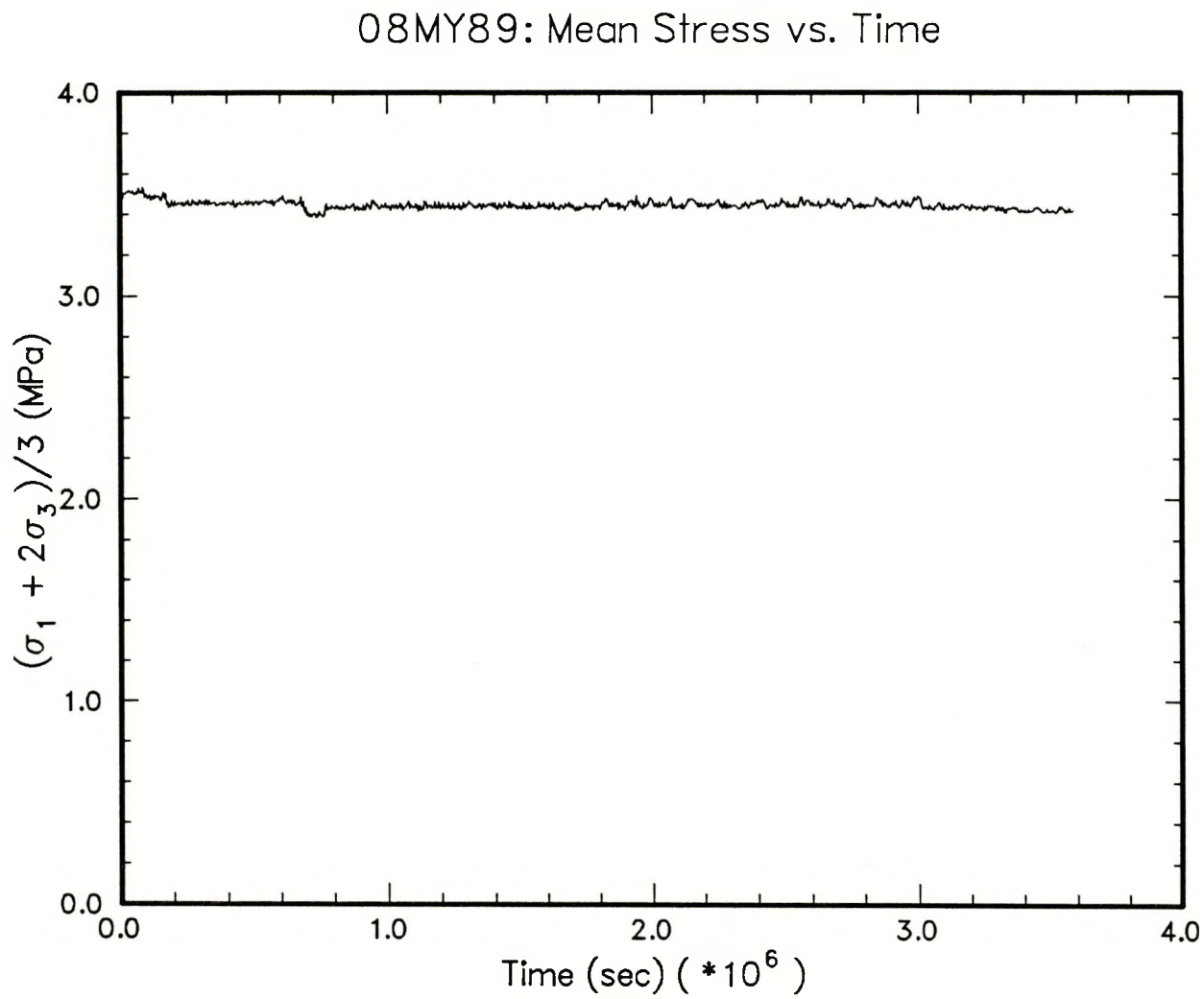

Figure 1: Plot of mean stress *versus* time for shear–consolidation experiment **08MY89**.

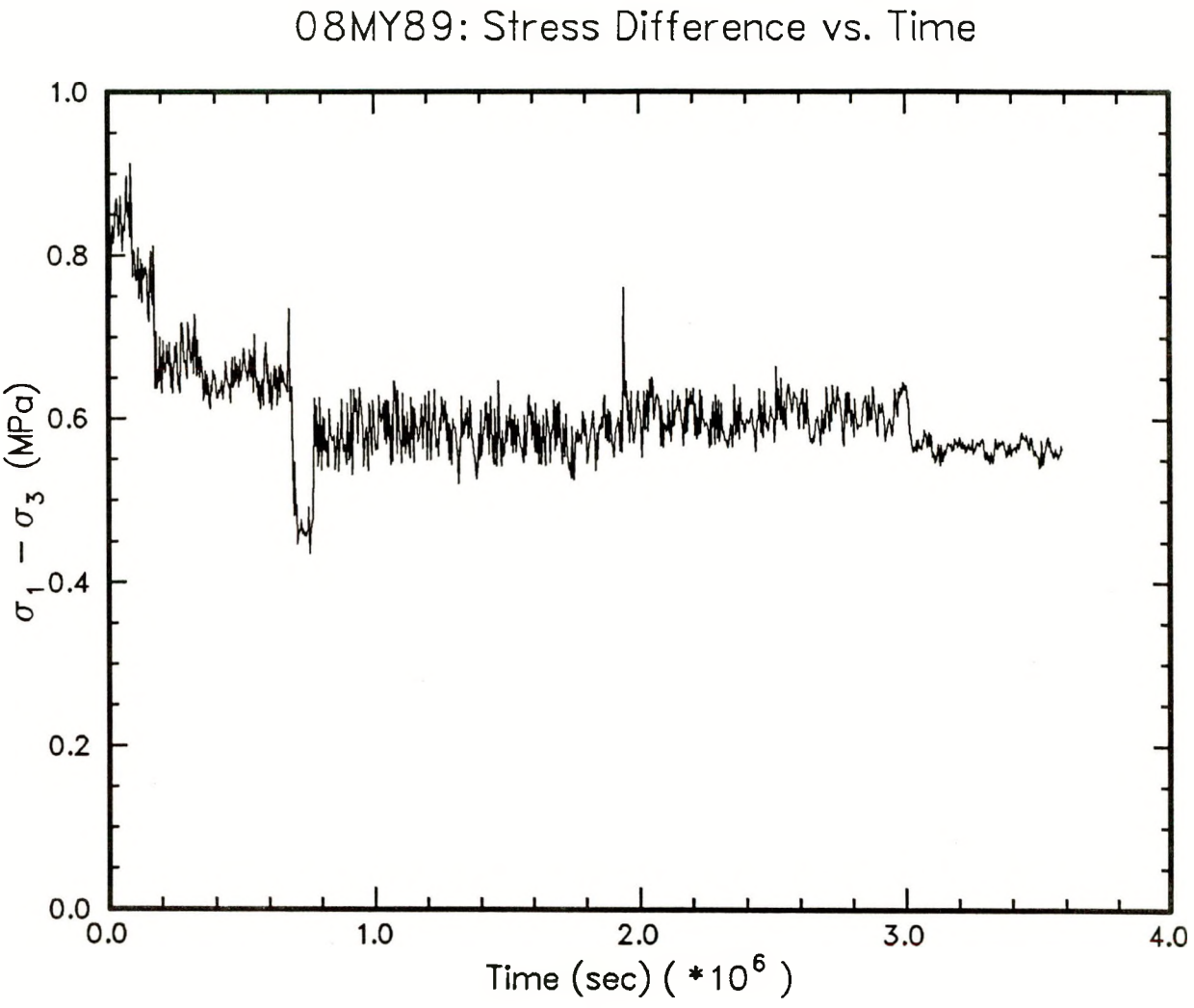

Figure 2: Plot of stress difference *versus* time for shear–consolidation experiment **08MY89**.

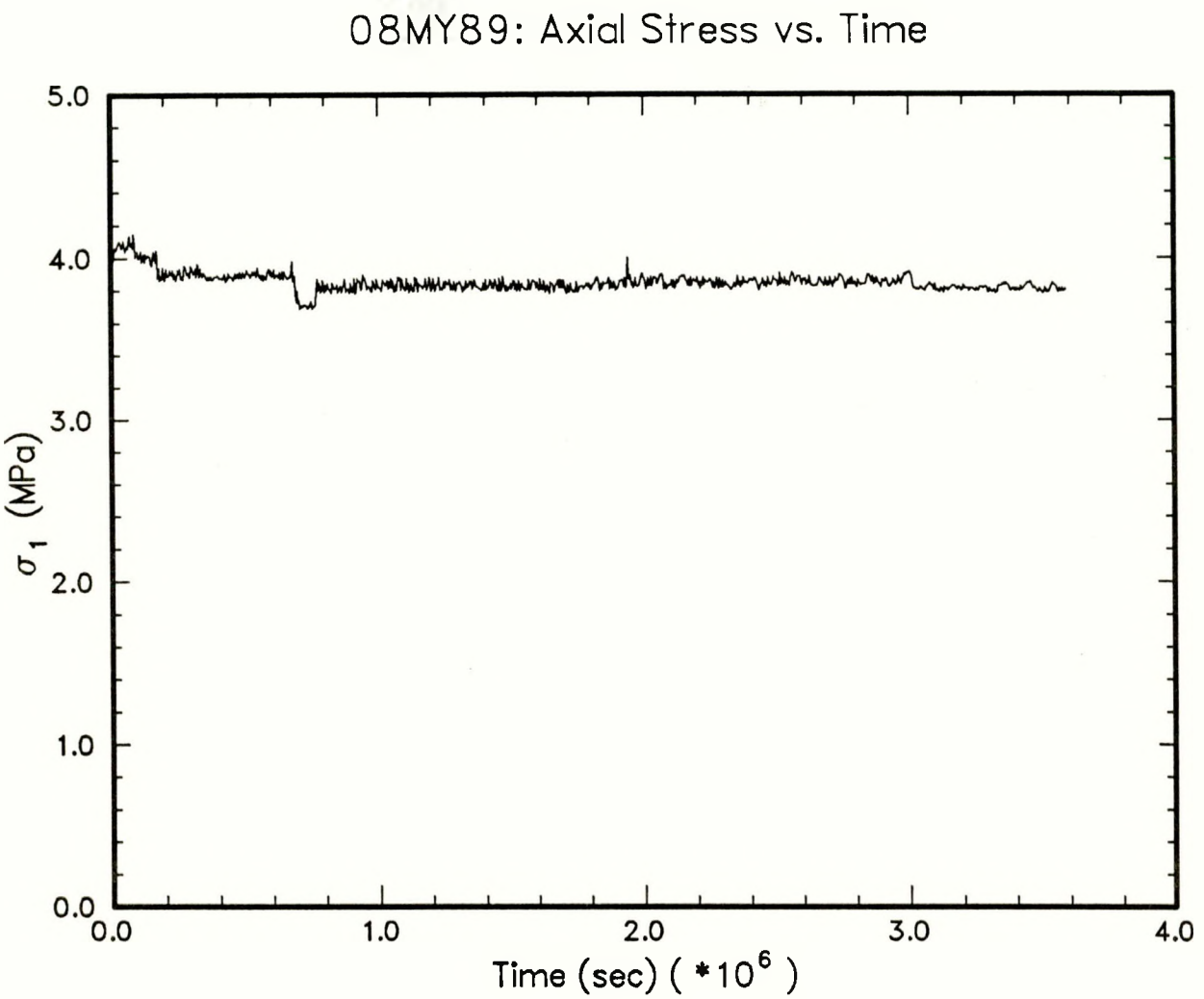

Figure 3: Plot of axial stress *versus* time for shear–consolidation experiment **08MY89**.

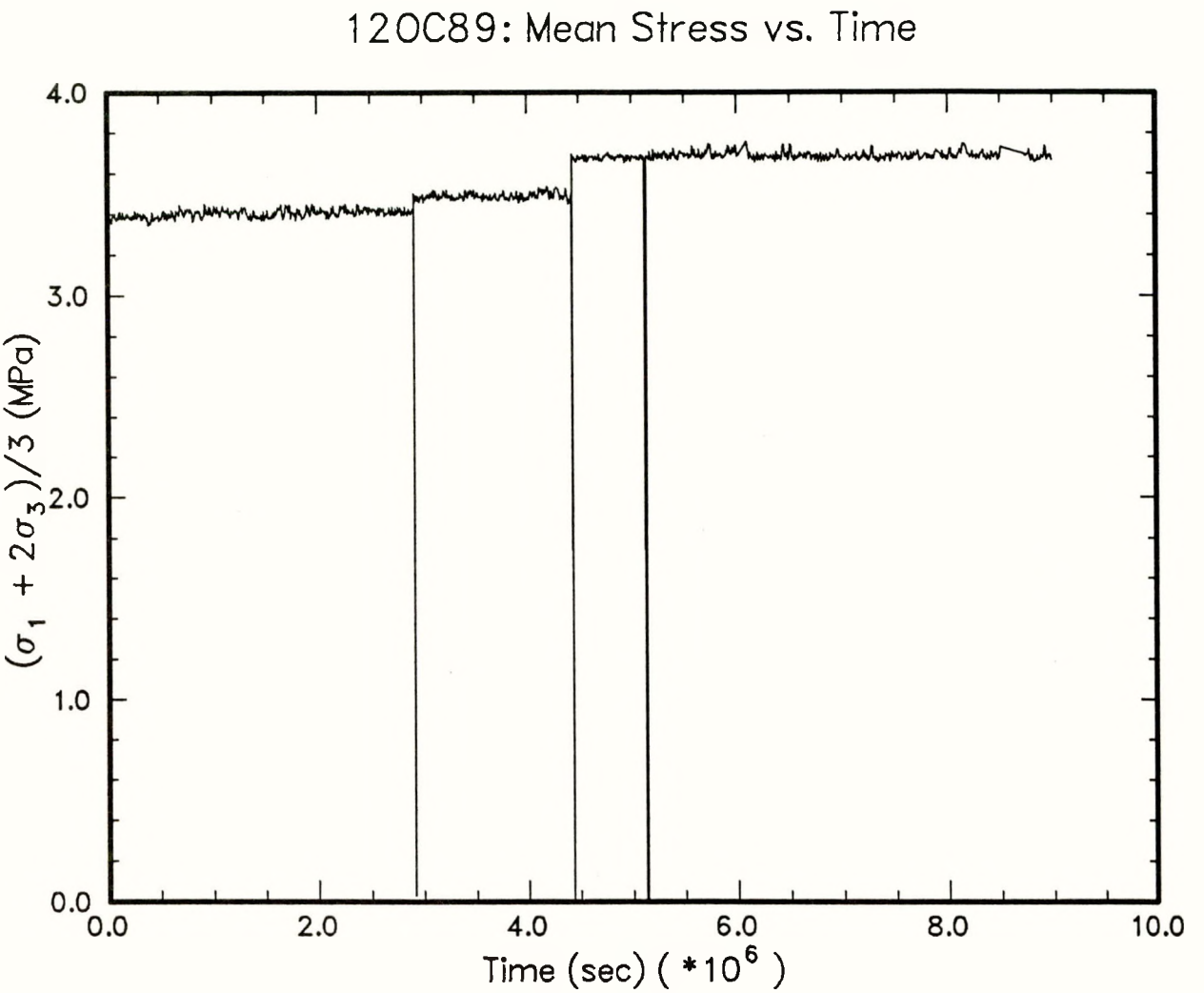

Figure 4: Plot of mean stress *versus* time for shear–consolidation experiment **12OC89**.

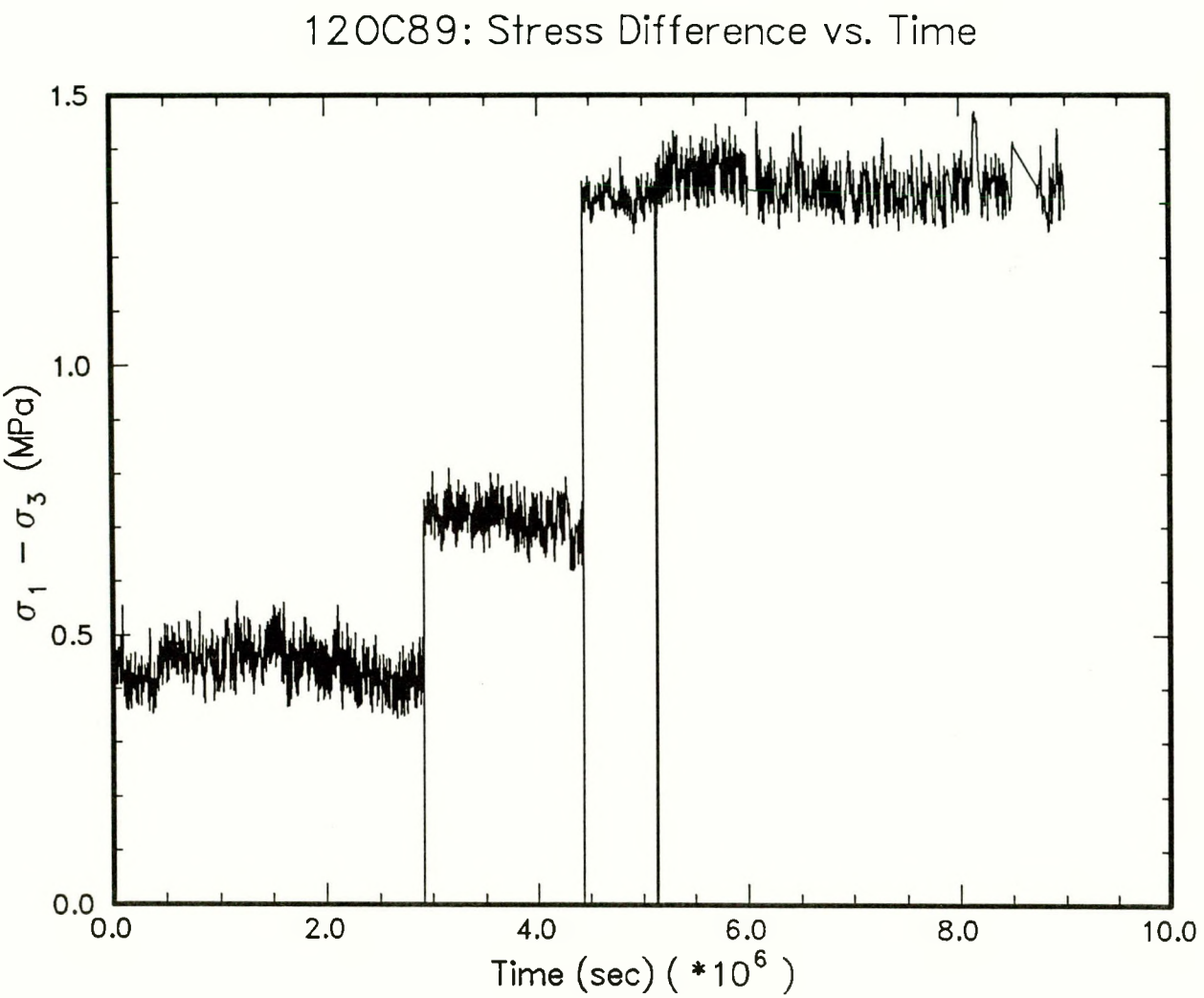

Figure 5: Plot of stress difference *versus* time for shear–consolidation experiment **12OC89**.

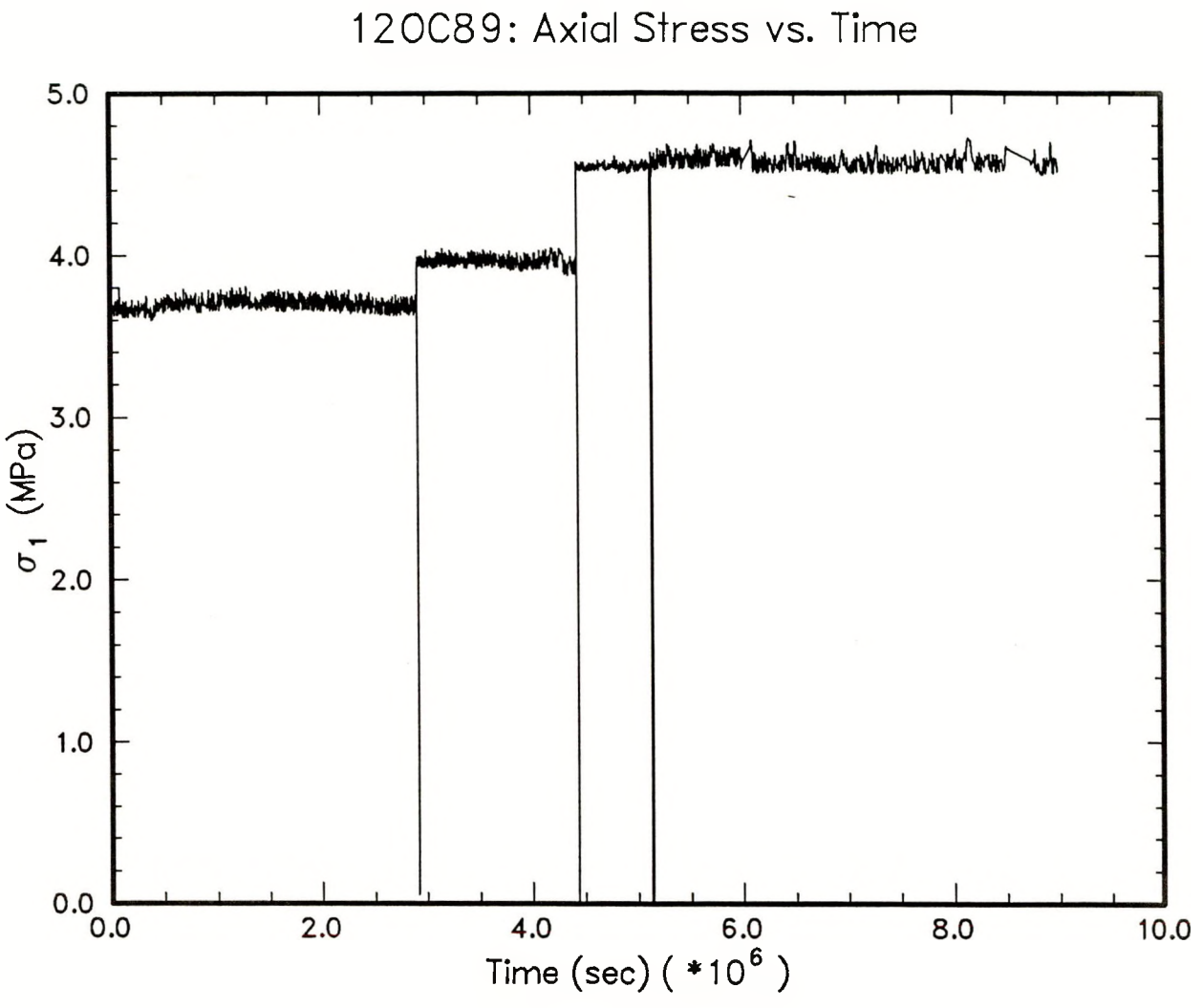

Figure 6: Plot of axial stress *versus* time for shear–consolidation experiment **12OC89**.

DISTRIBUTION

UC-721 (531)

FEDERAL AGENCIES

U. S. Department of Energy, (5)
Office of Civilian Radioactive Waste Management
Attn: Deputy Director, RW-2
Associate Director, RW-10
Office of Program Administration and Resources Management
Associate Director, RW-20
Office of Facilities Siting and Development
Associate Director, RW-30
Office of Systems Integration and Regulations
Associate Director, RW-40
Office of External Relations and Policy
Forrestal Building
Washington, DC 20585

U. S. Department of Energy (3)
Albuquerque Operations Office
Attn: J. E. Bickel
R. Marquez, Director
Public Affairs Division
P.O. Box 5400
Albuquerque, NM 87185

U. S. Department of Energy
Attn: National Atomic Museum Library
Albuquerque Operations Office
P. O. Box 5400
Albuquerque, NM 87185

U. S. Department of Energy (4)
WIPP Project Office (Carlsbad)
Attn: Vernon Daub
J. A. Mewhinney
D. C. Blackstone
J. E. Carr
R. Batra
P.O. Box 3090
Carlsbad, NM 88221

U. S. Department of Energy
Research & Waste Management Division
Attn: Director
P. O. Box E
Oak Ridge, TN 37831
U.S. Department of Energy
Waste Management Division
Attn: R. F. Guercia
P. O. Box 550
Richland, WA 99352

U. S. Department of Energy (1)
Attn: Edward Young
Room E-178
GAO/RCED/GTN
Washington, DC 20545

U. S. Department of Energy (6)
Office of Environmental Restoration and Waste Management
Attn: Jill Lytle, EM30
Mark Frei, EM-34 (3)
Mark Duff, EM-34
Clyde Frank, EM-50
Washington, DC 20585

U. S. Department of Energy (3)
Office of Environment, Safety and Health
Attn: Ray Pelletier, EH-231
Kathleen Taimi, EH-232
Carol Borgstrom, EH-25
Washington, DC 20585

U. S. Department of Energy (2)
Idaho Operations Office
Fuel Processing and Waste Management Division
785 DOE Place
Idaho Falls, ID 83402

U.S. Department of Energy
Savannah River Operations Office
Defense Waste Processing Facility Project Office
Attn: W. D. Pearson
P.O. Box A
Aiken, SC 29802

U.S. Environmental Protection Agency (2)
Attn: Ray Clark
Office of Radiation Programs (ANR-460)
Washington, DC 20460

U.S. Geological Survey
Branch of Regional Geology
Attn: R. Snyder
MS913, Box 25046
Denver Federal Center
Denver, CO 80225

U.S. Geological Survey
Conservation Division
Attn: W. Melton
P.O. Box 1857
Roswell, NM 88201

U.S. Geological Survey (2)
Water Resources Division
Attn: Kathy Peter
Suite 200
4501 Indian School, NE
Albuquerque, NM 87110

U.S. Nuclear Regulatory Commission (4)
Attn: Joseph Bunting, HLEN 4H3 OWFN
Ron Ballard, HLGP 4H3 OWFN
Jacob Philip
NRC Library
Mail Stop 623SS
Washington, DC 20555

BOARDS

Defense Nuclear Facilities Safety Board
Attn: Dermot Winters
Suite 700
625 Indiana Ave., NW
Washington, DC 20004

U. S. Department of Energy
Advisory Committee on Nuclear Facility Safety
Attn: Merritt E. Langston, AC21
Washington, DC 20585

Nuclear Waste Technical Review Board (2)
Attn: Dr. Don A. Deere
Dr. Sidney J. S. Parry
Suite 910
1100 Wilson Blvd.
Arlington, VA 22209-2297

Richard Major
Advisory Committee on Nuclear Waste
Nuclear Regulatory Commission
7920 Norfolk Avenue
Bethesda, MD 20814

STATE AGENCIES

Environmental Evaluation Group (3)
Attn: Library
Suite F-2
7007 Wyoming Blvd., N.E.
Albuquerque, NM 87109

New Mexico Bureau of Mines and Mineral Resources (2)
Attn: F. E. Kottolowski, Director
J. Hawley
Socorro, NM 87801

NM Department of Energy & Minerals
Attn: Librarian
2040 S. Pacheco
Santa Fe, NM 87505

NM Environmental Improvement Division
Attn: Deputy Director
1190 St. Francis Drive
Santa Fe, NM 87503

LABORATORIES/CORPORATIONS

Battelle Pacific Northwest Laboratories (5)
Attn: D. J. Bradley, K6-24
J. Relyea, H4-54
R. E. Westerman, P8-37
H. C. Burkholder, P7-41
L. Pederson, K6-47
Battelle Boulevard
Richland, WA 99352

Savannah River Laboratory (6)
Attn: N. Bibler
E. L. Albenisius
M. J. Plodinec
G. G. Wicks
C. Jantzen
J. A. Stone
Aiken, SC 29801

George Dymmel
SAIC
101 Convention Center Dr.
Las Vegas, NV 89109

INTERA Technologies, Inc. (4)
Attn: G. E. Grisak
J. F. Pickens
A. Haug
A. M. LeVenue
Suite #300
6850 Austin Center Blvd.
Austin, TX 78731

INTERA Technologies, Inc.
Attn: Wayne Stensrud
P.O. Box 2123
Carlsbad, NM 88221

IT Corporation (2)
Attn: R. F. McKinney
J. Myers
J. Valdez
D. Vetter
M. Abashian
Regional Office - Suite 700
5301 Central Avenue, NE
Albuquerque, NM 87108

IT Corporation (2)
Attn: D. E. Deal
P.O. Box 2078
Carlsbad, NM 88221

Los Alamos Scientific Laboratory
Attn: B. Erdal, CNC-11
Los Alamos, NM 87545

RE/SPEC, Inc.
Attn: W. Coons
P. F. Gnirk
Suite 300
4775 Indian School Rd., NE
Albuquerque NM 87110-3927

RE/SPEC, Inc. (7)
Attn: L. L. Van Sambeek
G. Callahan
T. Pfeifle
J. L. Ratigan
N. S. Brodsky
P. O. Box 725
Rapid City, SD 57709

Center for Nuclear Waste
Regulatory Analysis (4)
Attn: P. K. Nair
Southwest Research Institute
6220 Culebra Road
San Antonio, TX 78228-0510

Science Applications
International Corporation
Attn: Howard R. Pratt,
Senior Vice President
10260 Campus Point Drive
San Diego, CA 92121

Science Applications
International Corporation
Attn: Michael B. Gross
Ass't. Vice President
Suite 1250
160 Spear Street
San Francisco, CA 94105

Science Applications
International Corporation
Attn: T. W. Thompson
Suite 255
14062 Denver West Parkway
Golden, CO 80401

Systems, Science, and Software (2)
Attn: E. Peterson
Box 1620
La Jolla, CA 92038

Westinghouse Electric Corporation (7)
Attn: Library
Lamar Trego
W. P. Poirer
W. R. Chiquelin
V. F.Likar
D. J. Moak
R. F. Kehrman
P. O. Box 2078
Carlsbad, NM 88221

Weston Corporation (1)
Attn: David Lechel
Suite 1000
5301 Central Avenue, NE
Albuquerque, NM 87108

UNIVERSITIES

University of Arizona
Attn: J. G. McCray
Department of Nuclear Engineering
Tucson, AZ 85721

University of New Mexico (2)
Geology Department
Attn: D. G. Brookins
Library
M. Jercinivic
Albuquerque, NM 87131

Pennsylvania State University
Materials Research Laboratory
Attn: Della Roy
University Park, PA 16802

Texas A&M University
Center of Tectonophysics
College Station, TX 77840

G. Ross Heath
College of Ocean
and Fishery Sciences
University of Washington
Seattle, WA 98195

Dr. Howard Adler
Oak Ridge Associated Universities
Medical Science Division
P. O. Box 117
Oak Ridge, TN 37831-0117

INDIVIDUALS

Dennis W. Powers
Star Route Box 87
Anthony, TX 79821

LIBRARIES

Thomas Brannigan Library
Attn: Don Dresp, Head Librarian
106 W. Hadley St.
Las Cruces, NM 88001

Hobbs Public Library
Attn: Ms. Marcia Lewis, Librarian
509 N. Ship Street
Hobbs, NM 88248

New Mexico State Library
Attn: Ms. Ingrid Vollenhofer
P.O. Box 1629
Santa Fe, NM 87503

New Mexico Tech
Martin Speere Memorial Library
Campus Street
Socorro, NM 87810

Pannell Library
Attn: Ms. Ruth Hill
New Mexico Junior College
Lovington Highway
Hobbs, NM 88240

WIPP Public Reading Room
Attn: Director
Carlsbad Public Library
101 S. Halagueno St.
Carlsbad, NM 88220

Government Publications Department
General Library
University of New Mexico
Albuquerque, NM 87131

THE SECRETARY'S BLUE RIBBON PANEL ON WIPP

Dr. Thomas Bahr
New Mexico Water Resources Institute
New Mexico State University
Box 3167
Las Cruces, NM 88003-3167

Mr. Leonard Slosky
Slosky and Associates
Suite 1400
Bank Western Tower
1675 Tower
Denver, Colorado 80202

Mr. Newal Squyres
Holland & Hart
P. O. Box 2527
Boise, Idaho 83701

Dr. Arthur Kubo
Vice President
BDM International, Inc.
7915 Jones Branch Drive
McLean, VA 22102

Mr. Robert Bishop
Nuclear Management Resources Council
Suite 300
1776 I Street, NW
Washington, DC 20006-2496

NATIONAL ACADEMY OF SCIENCES, WIPP PANEL

Dr. Charles Fairhurst, Chairman
Department of Civil and Mineral Engineering
University of Minnesota
500 Pillsbury Dr. SE
Minneapolis, MN 55455-0220

Dr. John O. Blomeke
Route 3
Sandy Shore Drive
Lenoir City, TN 37771

Dr. John D. Bredehoeft
Western Region Hydrologist
Water Resources Division
U.S. Geological Survey (M/S 439)
345 Middlefield Road
Menlo Park, CA 94025

Dr. Karl P. Cohen
928 N. California Avenue
Palo Alto, CA 94303

Dr. Fred M. Ernsberger
250 Old Mill Road
Pittsburgh, PA 15238

Dr. Rodney C. Ewing
Department of Geology
University of New Mexico
200 Yale, NE
Albuquerque, NM 87131

B. John Garrick
Pickard, Lowe & Garrick, Inc.
2260 University Drive
Newport Beach, CA 92660

Leonard F. Konikow
U.S. Geological Survey
431 National Center
Reston, VA 22092

Jeremiah O'Driscoll
505 Valley Hill Drive
Atlanta, GA 30350

Dr. Christopher G. Whipple
Clement International
Suite 1380
160 Spear Street
San Francisco, CA 94105

Dr. Peter B. Myers, Staff Director
National Academy of Sciences
Committee on Radioactive Waste Management
2101 Constitution Avenue
Washington, DC 20418

Dr. Geraldine Grube
Board on Radioactive Waste Management
GF456
2101 Constitution Avenue
Washington, DC 20418

FOREIGN ADDRESSES

Studiecentrum Voor Kernenergie
Centre D'Energie Nucleaire
Attn: Mr. A. Bonne
SCK/CEN
Boeretang 200
B-2400 Mol
BELGIUM

Atomic Energy of Canada, Ltd. (2)
Whiteshell Research Estab.
Attn: Peter Haywood
John Tait
Pinewa, Manitoba, CANADA
ROE 1LO

Dr. D. K. Mukerjee
Ontario Hydro Research Lab
800 Kipling Avenue
Toronto, Ontario, CANADA
M8Z 5S4

Mr. Francois Chenevier, Director (2)
ANDRA
Route du Panorama Robert Schumann
B.P.38
92266 Fontenay-aux-Roses Cedex
FRANCE

Mr. Jean-Pierre Olivier
OECD Nuclear Energy Agency
Division of Radiation Protection
and Waste Management
38, Boulevard Suchet
75016 Paris, FRANCE

Claude Sombret
Centre D'Etudes Nucleaires
De La Vallee Rhone
CEN/VALRHO
S.D.H.A. BP 171
30205 Bagnols-Sur-Ceze
FRANCE

Bundesministerium fur Forschung und
Technologie
Postfach 200 706
5300 Bonn 2
FEDERAL REPUBLIC OF GERMANY

Bundesanstalt fur Geowissenschaften
und Rohstoffe
Attn: Michael Langer
Postfach 510 153
3000 Hannover 51
FEDERAL REPUBLIC OF GERMANY

Hahn-Meitner-Institut fur
Kernforschung
Attn: Werner Lutze
Glienicker Strasse 100
100 Berlin 39
FEDERAL REPUBLIC OF GERMANY

Institut fur Tieflagerung (4)
Attn: K. Kuhn
Theodor-Heuss-Strasse 4
D-3300 Braunschweig
FEDERAL REPUPLIC OF GERMANY

Kernforschug Karlsruhe
Attn: K. D. Closs
Postfach 3640
7500 Karlsruhe
FEDERAL REPUBLIC OF GERMANY

Physikalisch-Technische Bundesanstalt
Attn: Peter Brenneke
Postfach 33 45
D-3300 Braunschweig
FEDERAL REPUBLIC OF GERMANY

D. R. Knowles
British Nuclear Fuels, plc
Risley, Warrington, Cheshire WA3 6AS
1002607 GREAT BRITAIN

Shingo Tashiro
Japan Atomic Energy Research
Institute
Tokai-Mura, Ibaraki-Ken
319-11 JAPAN

Netherlands Energy Research
Foundation ECN (2)
Attn: Tuen Deboer, Mgr.
L. H. Vons
3 Westerduinweg
P.O. Box 1
1755 ZG Petten, THE NETHERLANDS

Svensk Karnbransleforsorjning AB
Attn: Fred Karlsson
Project KBS
Karnbranslesakerhet
Box 5864
10248 Stockholm, SWEDEN

SANDIA INTERNAL

400 L. D. Tyler
1510 J. C. Cummings
1514 H. S. Morgan
1514 J. R. Weatherby
1514 C. M. Stone
1514 J. G. Arguello
1550 C. W. Peterson
3141 S. A. Landenberger (5)
3151 G. C. Claycomb (3)
3145 Document Control (8)
for DOE/OSTI
6000 V. L. Dugan, Acting
6232 W. R. Wawersik
6232 D. H. Zeuch (10)
6232 W. A. Olsson
6232 D. J. Holcomb
6232 D. J. Zimmerer
6233 J. C. Eichelberger
6233 J. L. Krumhansl
6300 T. O Hunter, Acting
6310 T. E. Blejwas, Acting
6313 L. E. Shephard
6315 M. D. Siegel
6340 W. D. Weart
6340 S. Y. Pickering
6341 R. C. Lincoln
6341 Staff (9)
6341 Sandia WIPP Central Files (10)
6342 D. R. Anderson
6342 Staff (11)
6343 T. M. Schultheis
6343 Staff (2)
6344 E. Gorham
6344 Staff (10)
6345 B. M. Butcher, Acting (10)
6345 Staff (9)
6346 J. R. Tillerson
6346 Staff (7)
6620 J. C. Stormont (15)
7542 M. E. F. Shields
8523 R. C. Christman (SNLL Library)
9300 J. E. Powell
9310 J. D. Plimpton
9320 M. J. Navratil
9325 L. J. Keck (2)
9330 J. D. Kennedy
9333 O. Burchett
9333 J. W. Mercer
9334 P. D. Seward

Org.	Bldg.	Name	Rec'd by	Org.	Bldg.	Name	Rec'd by

Sandia National Laboratories